

The Plant Journal (2020) 101, 1152-1169

doi: 10.1111/tpj.14581

# Expression of a dominant-negative AtNEET-H89C protein disrupts iron-sulfur metabolism and iron homeostasis in Arabidopsis

Sara I. Zandalinas<sup>1</sup> (D), Luhua Song<sup>2</sup>, Soham Sengupta<sup>2</sup> (D), Samuel A. McInturf<sup>1</sup>, DeAna G. Grant<sup>3</sup>, Henri-Baptiste Marjault<sup>4</sup>, Norma A. Castro-Guerrero<sup>1</sup>, David Burks<sup>2</sup>, Rajeev K. Azad<sup>2</sup>, David G. Mendoza-Cozatl<sup>1</sup> (D), Rachel Nechushtai<sup>4</sup> and Ron Mittler<sup>1,5,\*</sup> (D)

Received 12 April 2019; revised 4 October 2019; accepted 16 October 2019; published online 23 October 2019. \*For correspondence (e-mail mittlerr@missouri.edu).

#### **SUMMARY**

Iron–sulfur (Fe–S) clusters play an essential role in plants as protein cofactors mediating diverse electron transfer reactions. Because they can react with oxygen to form reactive oxygen species (ROS) and inflict cellular damage, the biogenesis of Fe–S clusters is highly regulated. A recently discovered group of 2Fe–2S proteins, termed NEET proteins, was proposed to coordinate Fe–S, Fe and ROS homeostasis in mammalian cells. Here we report that disrupting the function of AtNEET, the sole member of the NEET protein family in *Arabidopsis thaliana*, triggers leaf-associated Fe–S- and Fe-deficiency responses, elevated Fe content in chloroplasts (1.2–1.5-fold), chlorosis, structural damage to chloroplasts and a high seedling mortality rate. Our findings suggest that disrupting AtNEET function disrupts the transfer of 2Fe–2S clusters from the chloroplastic 2Fe–2S biogenesis pathway to different cytosolic and chloroplastic Fe–S proteins, as well as to the cytosolic Fe–S biogenesis system, and that uncoupling this process triggers leaf-associated Fe–S- and Fe-deficiency responses that result in Fe over-accumulation in chloroplasts and enhanced ROS accumulation. We further show that AtNEET transfers its 2Fe–2S clusters to DRE2, a key protein of the cytosolic Fe–S biogenesis system, and propose that the availability of 2Fe–2S clusters in the chloroplast and cytosol is linked to Fe homeostasis in plants.

Keywords: AtNEET, Arabidopsis thaliana, DRE2, iron-sulfur cluster, iron, reactive oxygen species.

## INTRODUCTION

Iron–sulfur (Fe–S) proteins play a central role in many different metabolic and regulatory pathways in plants (Balk and Pilon, 2011; Bernard *et al.*, 2013; Balk and Schaedler, 2014; Hu *et al.*, 2017; Lu, 2018; Przybyla-Toscano *et al.*, 2018). They originated under highly reducing conditions during early evolution and are sensitive to damage by reactive oxygen species (ROS; Lill, 2009; Boyd *et al.*, 2014; Andreini *et al.*, 2017; Sengupta *et al.*, 2018). The biogenesis and mobilization of Fe–S clusters within cells is therefore tightly

regulated, protected and compartmentalized. Although much is known about how Fe–S clusters are formed in the different cellular compartments of plants (Balk and Pilon, 2011; Balk and Schaedler, 2014; Hu *et al.*, 2017; Lu, 2018; Przybyla-Toscano *et al.*, 2018), less is known about how this process is coordinated between different organelles, plant tissues and cell types, and how it is regulated based on the availability and mobilization of Fe and S.

A newly discovered group of mammalian 2Fe-2S proteins, termed NEET proteins, was recently proposed to

<sup>&</sup>lt;sup>1</sup>Division of Plant Sciences, College of Agriculture Food and Natural Resources and Interdisciplinary Plant Group, Christopher S. Bond Life Sciences Center, University of Missouri, 1201 Rollins St, Columbia, MO 65211, USA, <sup>2</sup>Department of Biological Sciences, College of Science, University of North Texas, 1155 Union Circle #305220, Denton, TX

<sup>76203-5017,</sup> USA, <sup>3</sup>Electron Microscopy Core Facility, University of Missouri, W136 Veterinary Medicine Building 1600 East Rollins Street, Columbia, MO 65211, USA,

<sup>&</sup>lt;sup>4</sup>The Alexander Silberman Institute of Life Science, The Hebrew University of Jerusalem, Edmond J. Safra Campus at Givat Ram, Jerusalem 91904, Israel, and

<sup>&</sup>lt;sup>5</sup>Department of Surgery, University of Missouri School of Medicine, Christopher S. Bond Life Sciences Center University of Missouri, 1201 Rollins St, Columbia, MO 65211, USA

play an important role in mobilizing 2Fe-2S clusters from the mitochondria to the cytosol, linking the Fe-S biogenesis pathway of the mitochondria with that of the cytosol (Lipper et al., 2015; Tamir et al., 2015; Mittler et al., 2018; Sengupta et al., 2018). NEET proteins were also proposed to play a key metabolic and regulatory role in several different human diseases, including cancer, diabetes and neurodegeneration (Tamir et al., 2015; Mittler et al., 2018). The flowering plant Arabidopsis thaliana contains a single gene encoding a NEET protein (At5g51720), and the protein product of this gene, AtNEET, was previously proposed to play an important role in maintaining Fe and ROS homeostasis in Arabidopsis (Nechushtai et al., 2012). Knockdown mutants and RNAi lines with suppressed expression of AtNEET displayed early senescence and accumulated higher levels of Fe and ROS. In addition, AtNEET was shown to transfer its 2Fe-2S clusters to apo-Ferredoxin (FD), and was able to mimic the function of the mammalian NEET protein mitoNEET in human cells (Nechushtai et al., 2012). In addition to the mitochondria, AtNEET is also localized to the chloroplast in plants, and its expression is restricted to leaves (Su et al., 2013; Khan et al., 2018).

The main feature distinguishing NEET proteins, such as AtNEET, from many of their Fe-S protein counterparts is the coordinating structure of their 2Fe-2S clusters. In all NEET proteins the 2Fe-2S cluster is coordinated by three cysteines and one histidine, as opposed to four cysteines observed in other 2Fe-2S clusters (Tamir et al., 2015; Mittler et al., 2018; Sengupta et al., 2018). This coordination structure enables the cluster to be mobilized or shared (donated or accepted) with other Fe-S proteins (Nechushtai et al., 2012; Tamir et al., 2014). AtNEET, for example, can actively donate its clusters to FD (binds a classic 2Fe-2S cluster, coordinated by four Cys residues), but when the single histidine coordinating the cluster of AtNEET was mutated to cysteine (H89C), AtNEET becomes a highly stable Fe-S protein unable to donate its clusters to FD (Nechushtai et al., 2012).

Despite growing interest in the function of AtNEET in the 2Fe-2S biogenesis, mobilization and metabolism of plants (Nechushtai et al., 2012; Su et al., 2013; Lu, 2018; Przybyla-Toscano et al., 2018; Tissot et al., 2019), very little is currently known about the precise role AtNEET plays in regulating these processes. This is perhaps because of a lack of true knock-out mutants for AtNEET, suggesting that it is an essential gene. To advance the study of AtNEET function in plants, we therefore used a dominant-negative strategy to disrupt its function by overexpressing the highly stable H89C variant of AtNEET in Arabidopsis. This strategy has been successfully used in cancer cells to disrupt the function of NAF-1, a human NEET protein, by overexpressing its H114C high-cluster-stability variant (equivalent to the Arabidopsis H89C mutant in stabilizing the cluster; Nechushtai et al., 2012; Tamir et al., 2014; Darash-Yahana et al., 2016). In both H114C and H89C proteins, the 2Fe-2S classical cluster binding site of NEET proteins is mutated from 3Cys-1His, which has low cluster stability and can donate its clusters to acceptor proteins, to 4Cys that has high cluster stability and is unable to donate its clusters to acceptor proteins (Nechushtai et al., 2012; Darash-Yahana et al., 2016). Expression of the H114C NEET variant in cancer cells has dramatic effects, including the suppression of cancer cell growth, initiating the activation of cell death and enhancing the sensitivity of cancer cells to ROS (Darash-Yahana et al., 2016). The rationale for using a dominant-negative strategy is that NEET proteins such as AtNEET or NAF-1 are homodimers (Nechushtai et al., 2012; Tamir et al., 2014; Mittler et al., 2018), and expressing a mutated high-cluster-stability version of the gene in transgenic plants will either replace the entire homodimer with a dysfunctional homodimer or form an inactive heterodimer composed of one wild-type (WT) and one mutated subunit, disrupting the overall NEET protein function in cells (Darash-Yahana et al., 2016).

Here we show that disrupting AtNEET function in plants results in the transcriptional re-programming of several networks mediating ROS metabolism, Fe-S biogenesis and Fe-deficiency responses. Despite an accumulation of many transcripts encoding Fe-S proteins, the protein level of key Fe-S proteins, such as FD, declines and Fe accumulates at the whole-plant level, and particularly in chloroplasts. These changes are accompanied by chlorosis, severe structural damage to chloroplasts and a high mortality rate of seedlings. We further show that AtNEET transfers its 2Fe-2S cluster to DRE2, a key protein of the cytosolic Fe-S biogenesis system. Our findings suggest that disrupting AtNEET function disrupts the transfer of 2Fe-2S clusters from the chloroplastic 2Fe-2S biogenesis pathway to cytosolic and chloroplastic Fe-S proteins, and that the availability of 2Fe-2S clusters is linked to Fe homeostasis in plants.

#### **RESULTS**

## Construction and characterization of AtNEET and H89C plants

We recently attempted to use clustered regularly interspaced short palindromic repeats (CRISPR)/CRISPR-associated protein 9 (Cas9) to knock-out AtNEET function, but despite the introduction of a frame-shifting nucleotide at the N-terminal region of AtNEET, some protein was maintained (Figure S1; similar to Lalonde et al., 2017; Mou et al., 2017; Gapinske et al., 2018; Smith et al., 2018; Sui et al., 2018). To disrupt AtNEET function in plants we therefore used a dominant-negative strategy (Darash-Yahana et al., 2016). For this purpose, we generated transgenic plants expressing the H89C mutant under the control of

the cauliflower mosaic virus (CaMV) 35S promoter (H89C plants). As controls we generated transgenic plants expressing the WT AtNEET protein under the control of the CaMV 35S promoter (NEET plants). In contrast to overexpression of the WT NEET protein (NEET), overexpression of the H89C protein (H89C) was detrimental to plants. Of the 23 H89C primary transformants obtained, five died at the seedling stage, five had severe growth defects and six more had a reduced growth phenotype. We therefore focused our study on the two H89C lines with the highest expression level of H89C that were still viable (H89C #4-3 and H89C #11-7), and on two NEET lines with comparable

or higher protein expression levels to these H89C lines (NEET #5-4 and NEET #10-10; Figures 1 and 2a). In addition to the reduced growth phenotype, H89C lines bolted earlier compared with WT or NEET-overexpressing lines (Figure 1b) and displayed chlorosis, with a mortality rate of about 20% (Figure 2a).

To study the function of AtNEET and to better understand the growth suppression phenotype associated with H89C mutation, we conducted comparative transcriptomics analysis on 7 day-old seedlings (Figure 2). At this stage, H89C seedlings displayed severe phenotypes, including chlorosis and delayed growth, compared with WT or NEET

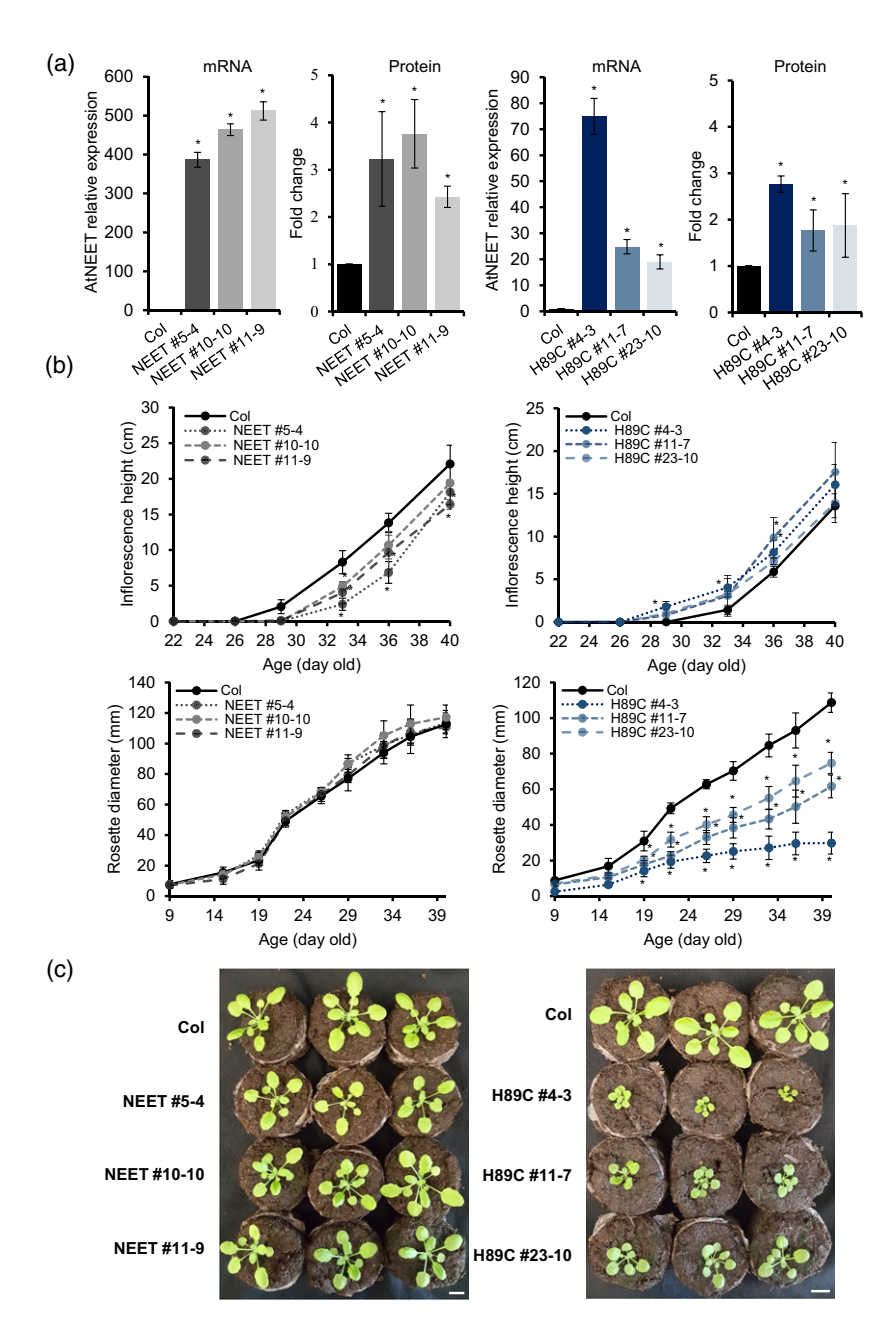


Figure 1. Expression of the H89C variant of AtNEET in transgenic plants stunts growth and triggers early bolting: (a) transcript and protein abundance of AtNEET and H89C; (b) rosette diameter and inflorescence height; and (c) images at day 21 of the three highest expressing AtNEET and H89C transgenic lines. Student test, SD, n=30, \*P<0.05. Scale bar in (c) indicates 1 cm. NEET, transgenic plants expressing AtNEET; H89C, transgenic plants expressing the H89C variant of AtNEET.

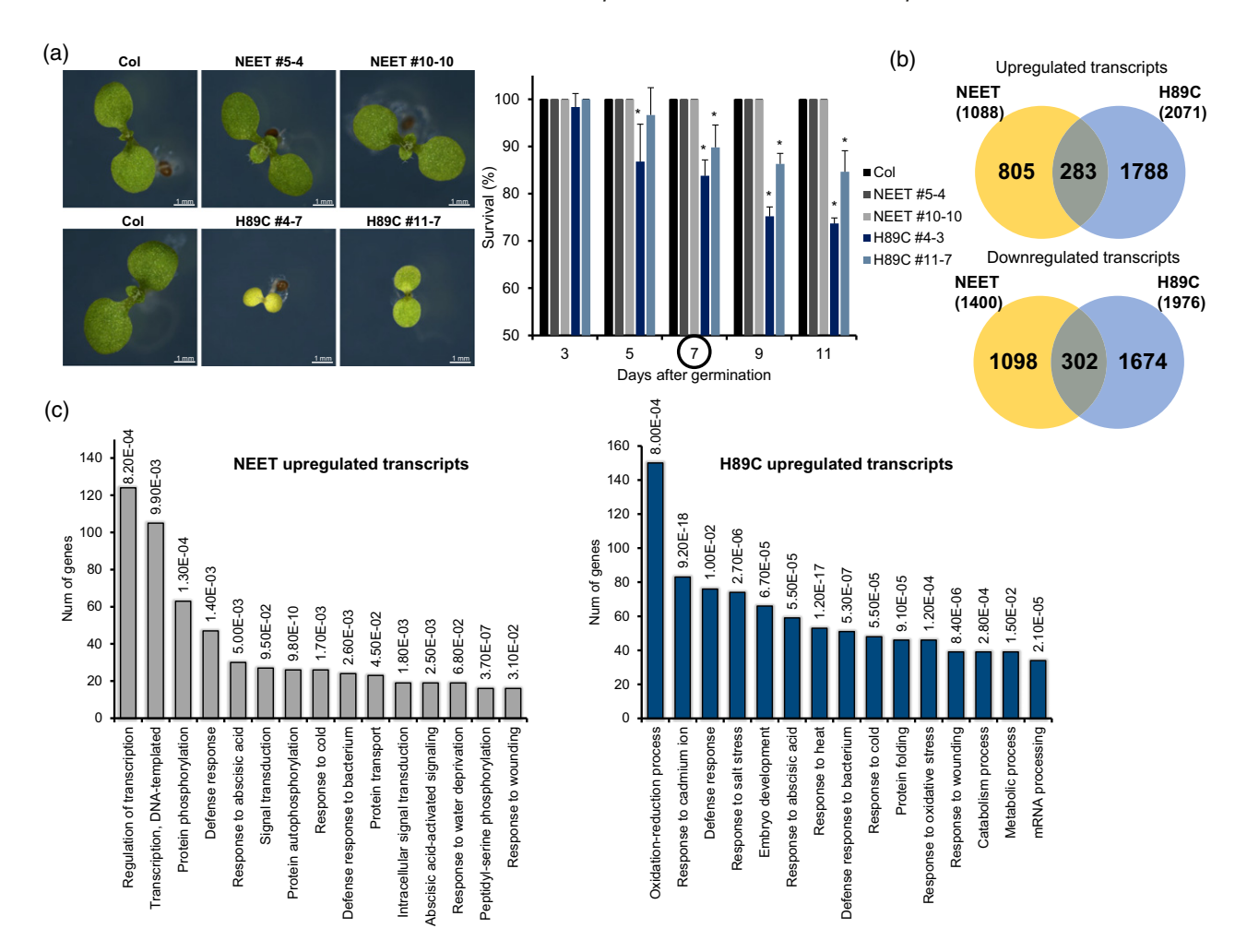


Figure 2. Seedling mortality and RNA-Seq analysis of transgenic plants expressing AtNEET or H89C. (a) Images (left) and a bar graph (right) showing the chlorotic appearance and mortality rate of seedlings expressing the H89C variant of AtNEET. (b) Venn diagrams showing the overlap between upregulated (top) or downregulated (bottom) transcripts in transgenic seedlings expressing AtNEET or H89C. (c) Gene ontology annotation of transcripts significantly upregulated in AtNEET or H89C plants (numbers above each bar represent P value for statistical significance). Student's t-test, SD, n = 30, \*P < 0.05. NEET, AtNEET-expressing seedlings; H89C, H89C variant of AtNEET-expressing seedlings.

(Figure 2a), and their mortality rate was 15% (the mortality rate of H89C seedlings could reach 20-25% by day 11; Figure 2a). Three biological replicates of each of the different H89C or NEET lines (H89C #4-3, H89C #11-7, NEET #5-4 and NEET #10-10), as well as three biological replicates of WT seedlings (each containing 80-100 seedlings), were subjected to RNA-Seg analysis. Overexpression of NEET resulted in the up- and downregulation of 1088 and 1400 transcripts, respectively (Tables S1 and S2), and overexpression of H89C resulted in the up- and downregulation of 2071 and 1976 transcripts, respectively (Tables S3 and S4; Figure 2b). Little overlap was found between transcripts significantly altered in NEET- or H89C-overexpressing plants, demonstrating that the single amino acid change between the overexpressed NEET and H89C proteins had a significant impact on plant metabolism and transcriptional programs (Figures 2b and S2). Transcripts

upregulated in NEET-overexpressing seedlings were primarily associated with transcription, protein phosphorylation and responses to pathogen, abscisic acid (ABA) and cold stress, whereas transcripts upregulated in H89C-overexpressing seedlings were primarily associated with oxidation-reduction processes, responses to cadmium, and responses to pathogen, ABA and salt stress (Figures 2c and S3). Notably, a substantial number (>10%) of transcripts associated with responses to hydrogen peroxide were also found in H89C plants (Table 1).

## Activation of ROS-response networks and the leaf Fedeficiency response in H89C plants

The presence of upregulated transcripts associated with the response of plants to hydrogen peroxide (Table 1), as well as oxidation-reduction processes (Figure 2c), in H89C plants prompted us to examine different transcription

Table 1 Response of transcripts significantly upregulated in AtNEET or H89C to different hormones and reactive oxygen species (ROS)

Hormone/ROS	1088 NEET	2071 H89C
ABA	79 (7.26%)	175 (8.45%)
ACC	2 (0.18%)	20 (0.96%)
Brassinolide	26 (2.38%)	13 (0.62%)
Cytokinin	44 (4.04%)	83 (4.01%)
Gibberellin	6 (0.55%)	7 (0.33%)
Indole-3-acetic acid	33 (3.03%)	32 (1.54%)
Methyl jasmonate	83 (7.62%)	151 (7.29%)
SA	14 (1.28%)	71 (3.42%)
$H_2O_2$	99 (9.09%)	244 (11.78%)
02-	21 (1.93%)	88 (4.24%)
<sub>1</sub> 0 <sup>2</sup>	43 (3.95%)	27 (1.3%)

Total number of significantly altered transcripts in NEET (1088) or H89C (2071) is indicated at the top. In bold, transcripts with more than 10% of representation. Abbreviations: ABA, abscisic acid; ACC, 1-aminocyclopropane-1-carboxylic acid; SA, salicylic acid.

factor (TF) networks associated with responses to ROS in H89C plants. As shown in Figure 3a,b, numerous ROS-response TFs and many of their associated transcripts were

found to be upregulated in H89C plants. These included ROS- and heat-response heat-shock transcription factors (HSFs; Ohama et al., 2017), stress- and pathogen-response WRKYs (Viana et al., 2018), and light- and stress-response TFs such as Zat12 (Davletova et al., 2005) and BRUTUS (BTS; an E3 ligase known to regulate Fe-deficiency responses, primarily induced in leaves during Fe deprivation; Le et al., 2016; Hindt et al., 2017). Moreover, in contrast to NEET-expressing seedlings, and compared with the WT, the accumulation of hydrogen peroxide was higher in H89C-expressing plants (Figure 3c). As shown in Figure 3(a), many of the ROS-response TFs upregulated in H89C plants were also upregulated in Arabidopsis seedlings in response to treatment with 1 mm H<sub>2</sub>O<sub>2</sub> (H<sub>2</sub>O<sub>2</sub>; Zandalinas et al., 2019). These findings further strengthen the link between H89C expression, H2O2 accumulation and oxidative stress.

The identification of zinc finger of *Arabidopsis* thaliana 12 (Zat12) and BTS among the upregulated transcripts associated with H89C expression (Figure 3) prompted us to examine the expression level of different transcripts associated with Fe deficiency and Fe

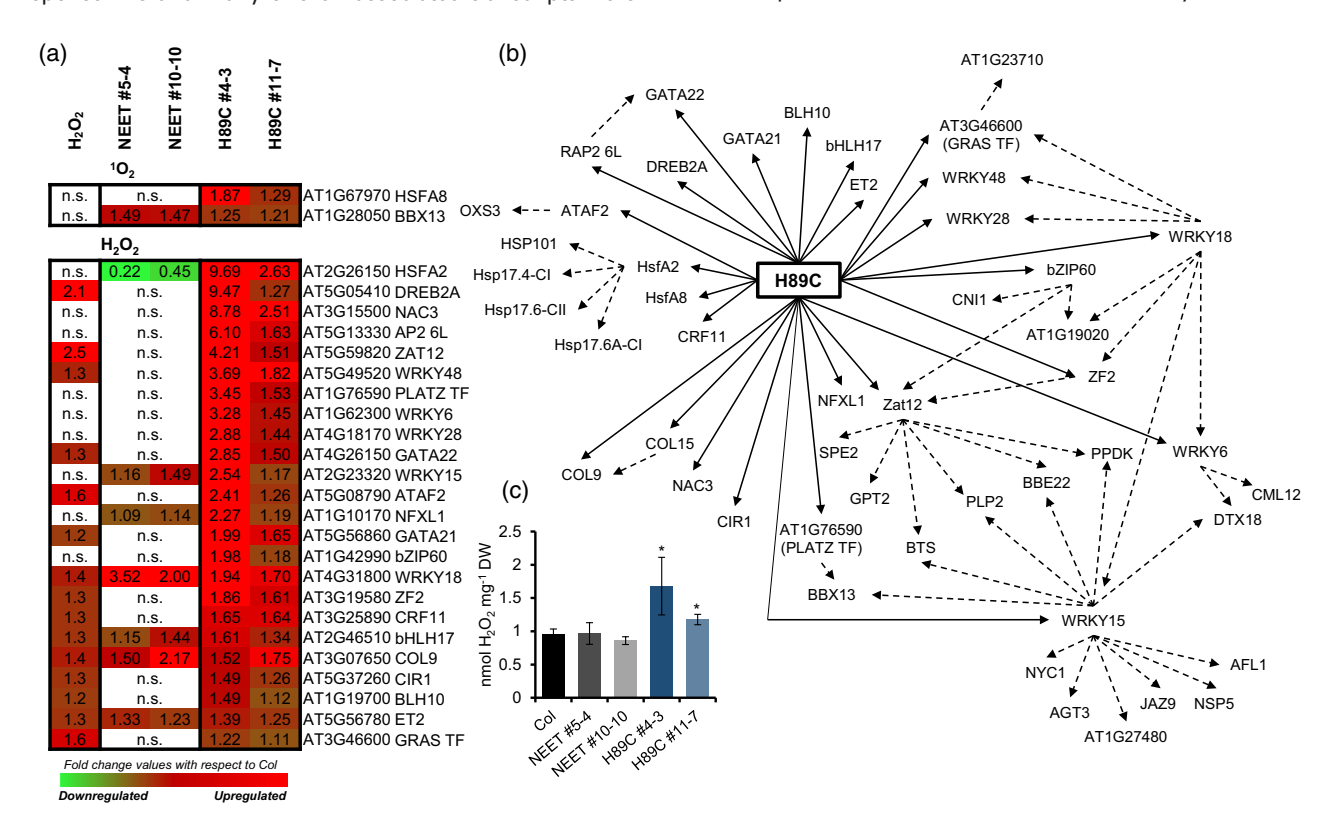


Figure 3. Expression of H89C results in the activation of reactive oxygen species (ROS) response transcription factors (TFs) and networks. (a) Heat map. (b) Expression association network for the different ROS-response TFs and some of their related targets significantly upregulated in seedlings expressing H89C. (c)  $H_2O_2$  content in wild type (Col), and AtNEET- and H89C-expressing seedlings. Significant transcripts compared with wild type (P < 0.05; ANOVA) are shown. Solid arrows indicate the significantly higher expression of different ROS-response TFs in H89C plants and dashed arrows indicate the potential activation of gene expression by the enhanced TFs of additional transcripts (based on previously published work; references provided in Appendix S1), also found to be upregulated in the data set for H89C plants. Student's *t*-test, SD, n = 5, \* P < 0.05. NEET, AtNEET-expressing seedlings; H89C, H89C variant of AtNEET-expressing seedlings; n.s., not significant; Please see Appendix S1 for additional abbreviations. Data for  $H_2O_2$ -associated transcripts ( $H_2O_2$ ) are from Zandalinas *et al.* (2019)

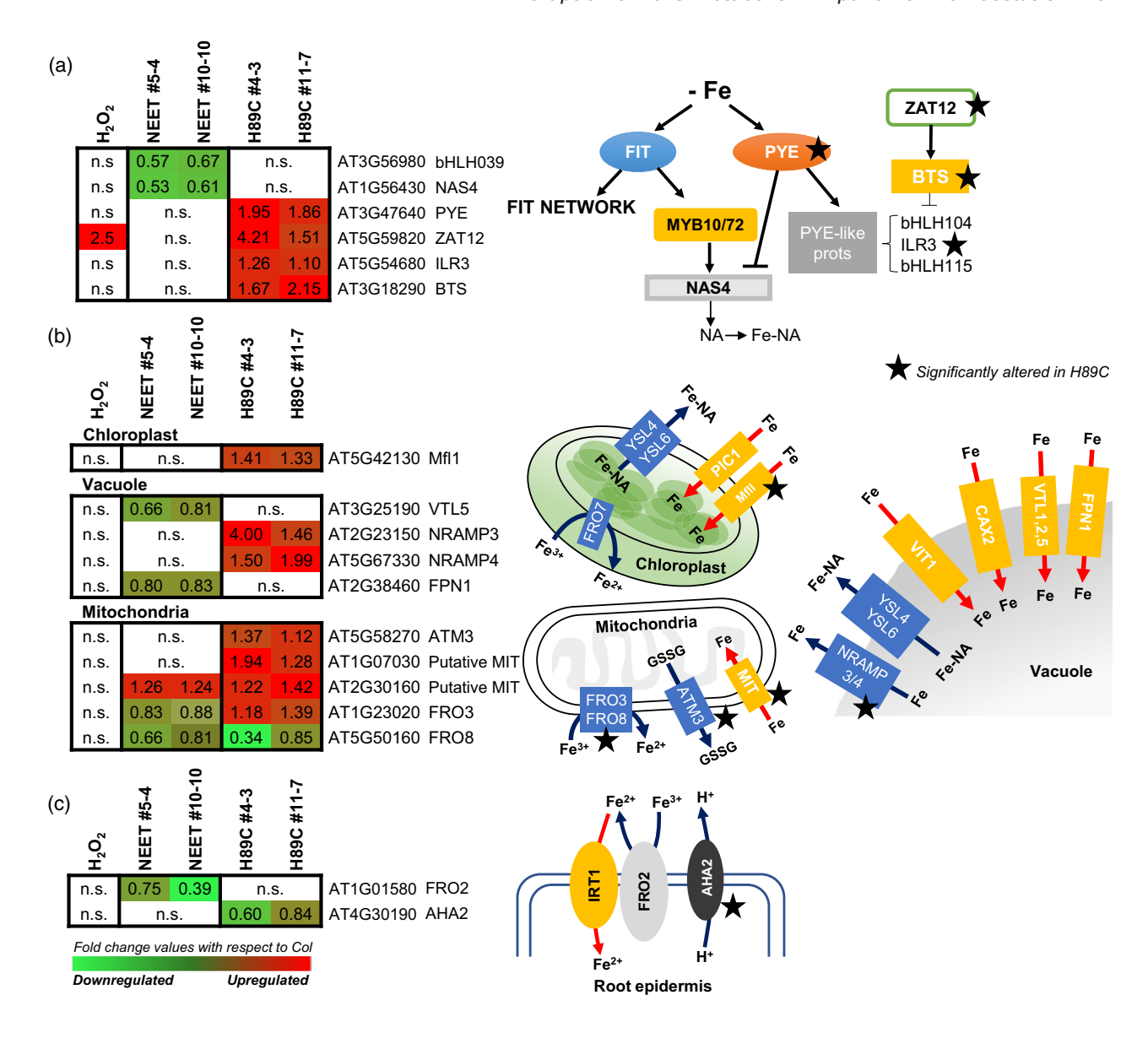


Figure 4. Expression of H89C results in the partial activation of the Fe-deficiency response. Heat maps (left) and models (right) of transcripts encoding: (a) selected Fe-deficiency response transcription factors; (b) Fe mobilization proteins in the chloroplast, vacuole and mitochondria; and (c) Fe mobilizing proteins and channels in the root. Significant transcripts compared with wild type (P < 0.05; ANOVA) are shown. NEET, AtNEET-expressing seedlings; H89C, H89C variant of AtNEET-expressing seedlings; n.s., not significant; Please see Appendix S1 for additional abbreviations. Data for H<sub>2</sub>O<sub>2</sub>-associated transcripts (H<sub>2</sub>O<sub>2</sub>) are from Zandalinas et al. (2019). Black stars indicate affected transcripts within each pathway.

accumulation in cells (Figure 4; Selote et al., 2015; Brumbarova et al., 2015; Le et al., 2016; Jeong et al., 2017; Khan et al., 2018; Kobayashi et al., 2019). Interestingly, the overexpression of H89C resulted in the upregulation of POPEYE (PYE), Zat12, IAA-leucine resistant 3 (ILR3) and BTS, which are components of the Fe-deficiency response known as the PYE network in Arabidopsis. In contrast, FIT (Fer-like Fe-deficiency induced transcription factor) and AHA2 (plasma membrane H<sup>+</sup>-ATPase 2), which are mostly associated with Fe-deficiency responses in roots, were not upregulated. In addition, transcripts encoding proteins involved in the mobilization of Fe into chloroplasts (MFL1) and mitochondria (MIT), and the mobilization of Fe from the vacuole to the cytosol (NRAMP3/4), were also upregulated in H89C (Figure 4). Most of these upregulated responses were not found in NEET-overexpressing plants. Taken together, our RNA-Seq analysis indicates that overexpression of H89C resulted in a partial activation of the Fe-deficiency response of Arabidopsis, primarily associated with leaves (Thomine and Vert, 2013; Brumbarova et al., 2015; Le et al., 2016; Jeong et al., 2017; Khan et al., 2018; Kobayashi et al., 2019). The activation of leaf-associated Fe-deficiency

responses in H89C plants (Figure 4) is also consistent with the expression pattern of AtNEET, which is restricted to green tissues (Khan *et al.*, 2018). Our results are also in agreement with the recent transcriptional link described for the bHLH factor ILR3 and AtNEET (Tissot *et al.*, 2019). Notably, and in contrast to the ROS-related transcripts upregulated in H89C plants (Figure 3), almost none of the Fe- (Figure 4) or Fe-S-related (Figure 5) transcripts upregulated in H89C plants were also upregulated in H<sub>2</sub>O<sub>2</sub>-treated seedlings (H<sub>2</sub>O<sub>2</sub>; Zandalinas *et al.*, 2019).

# Enhanced accumulation of transcripts encoding Fe-S biogenesis and Fe-S proteins in H89C plants

An Fe-deficiency response could be activated in plants if plants sense an increased demand to synthesize Fe-S clusters, as these two processes are thought to be linked (Hantzis et al., 2018). Such a need could arise if Fe-S biosynthesis and Fe-S mobilization are impaired by the overexpression of the H89C mutant, which is unable to donate its clusters. We therefore examined the expression levels of different transcripts associated with Fe-S biogenesis in the cytosol, mitochondria and chloroplast (Balk and Pilon, 2011; Bernard et al., 2013; Balk and Schaedler, 2014; Hu et al., 2017; Lu, 2018; Przybyla-Toscano et al., 2018). As shown in Figure 5(a), several transcripts associated with Fe-S biogenesis in all of these cellular compartments were upregulated in H89C-expressing plants but not in NEET-expressing plants. In addition, the expression of many transcripts encoding Fe-S proteins was upregulated in H89C plants (Figure 5b). The transcriptional responses shown in Figures 4 and 5 strongly suggest that the expression of H89C impaired Fe sensing and Fe-S homeostasis, inducing a transcriptional program consistent with Fe and Fe-S deficiency in plants.

# Decreased level of Fe-S proteins and damage to chloroplasts in H89C plants

To induce a state of Fe and Fe-S deficiency affecting the expression of different Fe-S pathways, as well as many Fe-S proteins, H89C would have to block at least some of the mobilization of Fe-S clusters between one or more Fe-S biogenesis pathways and Fe-S proteins, resulting in a decrease in the level of Fe-S proteins in cells. To test this possibility, we conducted an untargeted proteomics analysis of each of the different H89C or NEET lines (H89C #4-3, H89C #11-7, NEET #5-4 and NEET #10-10), as well as WT seedlings (three biological replicates each; 80-100 seedlings; 7 days old; Figures 5c, 6a and S4; Tables S5-S8). As shown in Figure 5(c), compared with control, the abundance of several Fe-S proteins was decreased in H89C plants. These included the chloroplastic proteins Ferredoxin 1 (FD1; 2Fe-2S) and a subunit of NAD(P)H dehydrogenase (NDHI; 4Fe-4S) that displayed significantly upregulated transcript levels

(Figure 5b) but lower protein abundance levels (Figure 5c). Interestingly, and in contrast to the decrease in Fe–S protein abundance, the level of several heme-containing proteins was not suppressed in H89C plants, and in some cases the abundance of the heme protein increased (Figure 5c). This finding suggested that 'free' Fe is not limiting and that the Fe-deficiency responses in H89C plants are primarily linked to the low availability of Fe–S clusters. The finding that the abundance of NDUS7 (NADH-ubiquinone oxidoreductase 20-kDa subunit, mitochondrial respiratory chain complex I) is enhanced in H89C plants (Figure 5c) could suggest that respiration is enhanced in H89C plants to compensate for the decrease in chloroplast function.

To further determine what group(s) of Fe-S proteins are primarily affected by H89C expression, we conducted a targeted proteomics analysis of different types of Fe-S proteins. As shown in Figure 5(d), H89C expression primarily reduced the expression of 2Fe-2S type Fe-S proteins, with no or marginal effect on other types of Fe-S proteins (3Fe-4S and 4Fe-4S). These findings suggest that AtNEET is primarily involved in 2Fe-2S metabolism. As shown in Figure 5d, only one 2Fe-2S protein in our analysis was found to be enhanced (PAO), and this may be because of the role this protein plays in chlorophyll catabolism, which correlates with the observed yellowing phenotype of the seedlings (Figure 2a). It is also possible that this protein receives its 2Fe-2S cluster in an AtNEET-independent manner. In addition, there is uncertainty as to the cluster type of SiRB, which could be a 4Fe-4S or a 2Fe-2S protein in vivo (Saha et al., 2012).

Our untargeted proteomics analysis of H89C seedlings (Figures 5c, 6a and S4; Tables S5-S8) further revealed a significant decrease in the abundance of many chloroplastic proteins. This finding correlated with a decrease in chlorophyll content (Figure 6b) and the appearance of chlorotic stunted seedlings (Figure 2a). To determine whether such an appearance was associated with a delay in chloroplast biogenesis or damage to chloroplasts, we conducted TEM analysis. As shown in Figure 6(c), expression of H89C was associated with the appearance of severely damaged chloroplasts that contained no starch granules and appeared highly distorted. In contrast to the appearance of chloroplasts, mitochondria and nuclei of leaves and roots appeared normal, suggesting that the expression of H89C primarily affects chloroplast function.

# Enhanced accumulation of iron in chloroplasts of H89C plants

Previously, it has been shown that reduced expression of AtNEET was associated with an enhanced accumulation of Fe in Arabidopsis plants (Nechushtai *et al.*, 2012). To test whether a similar phenomenon accompanied the

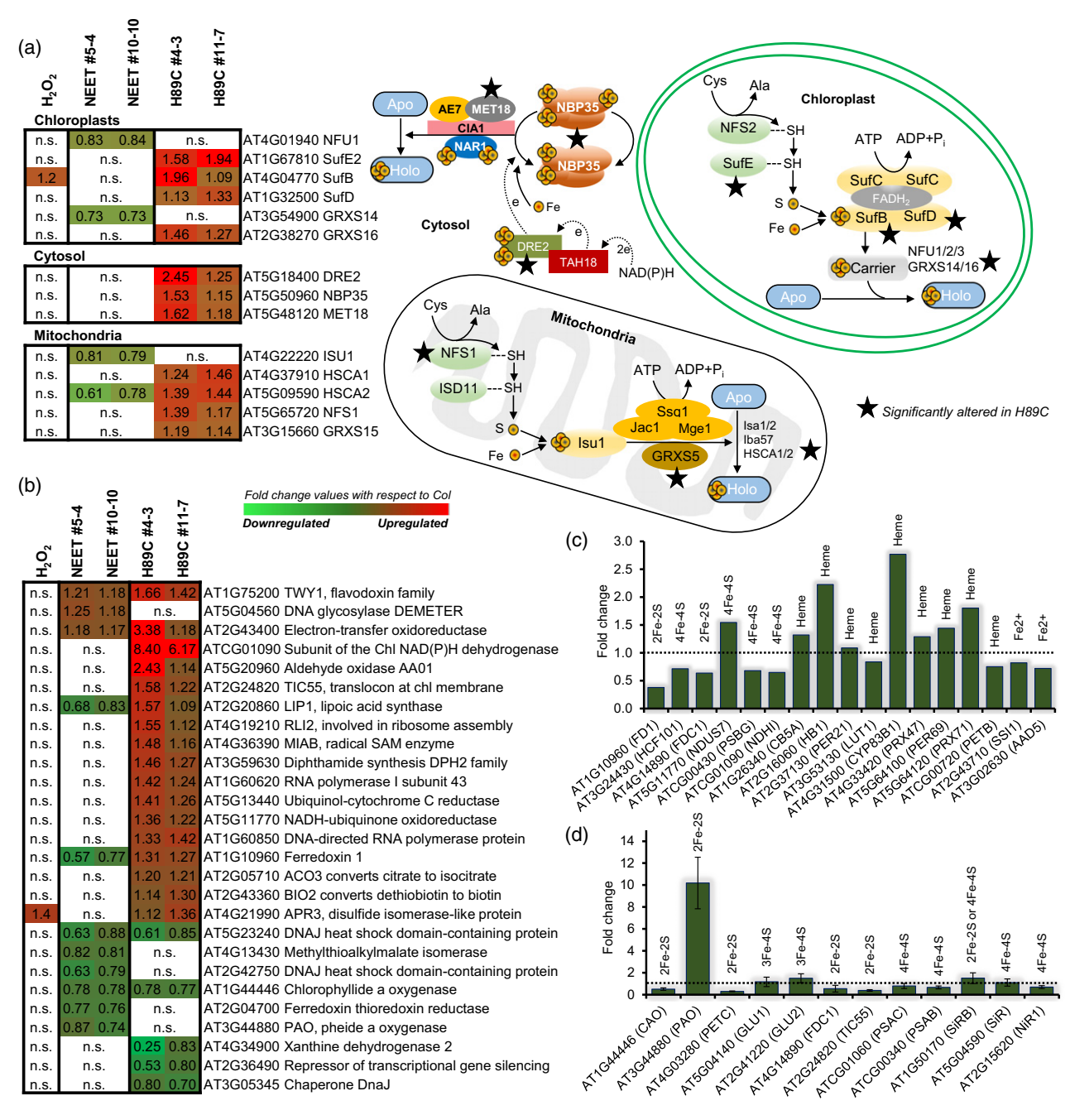


Figure 5. Expression of H89C impairs Fe-S metabolism. (a) Heat map (left) and models (right) showing the elevated expression of transcripts encoding Fe-S biogenesis pathways in H89C and AtNEET expressing seedlings. (b) Heat map showing the enhanced expression of transcripts encoding Fe-S proteins in H89C and AtNEET expressing seedlings. (c) Bar graph showing the abundance of Fe-S, heme and iron-containing proteins in H89C seedlings. (d) Bar graph showing the abundance of different Fe-S proteins determined by targeted proteomics. Significant transcripts and proteins compared to wild type (n = 6; P < 0.05; ANOVA followed by a Tukey post hoc test) are shown. NEET, AtNEET-expressing seedlings; H89C, H89C variant of AtNEET-expressing seedlings; n.s., not significant; Please see Appendix S1 for additional abbreviations. Data set for H<sub>2</sub>O<sub>2</sub>-associated transcripts (H<sub>2</sub>O<sub>2</sub>) is from Zandalinas et al. (2019). Black stars indicate affected transcripts within each pathway.

overexpression of H89C or NEET we measured total Fe levels in 7-day-old seedlings of WT, NEET and H89C plants. As shown in Figure 7, H89C plants accumulated more Fe compared with WT or NEET plants. This was evident based on both Pearl's staining (Figure 7a) and inductively

coupled plasma optical emission spectroscopy (ICP-OES) analysis of seedlings (Figure 7b). Moreover, the staining of light microscopy mounts and transmission electron microscopy (TEM) sections with Pearl's, as well as inductively coupled plasma mass spectrometry (ICP-MS) analysis of

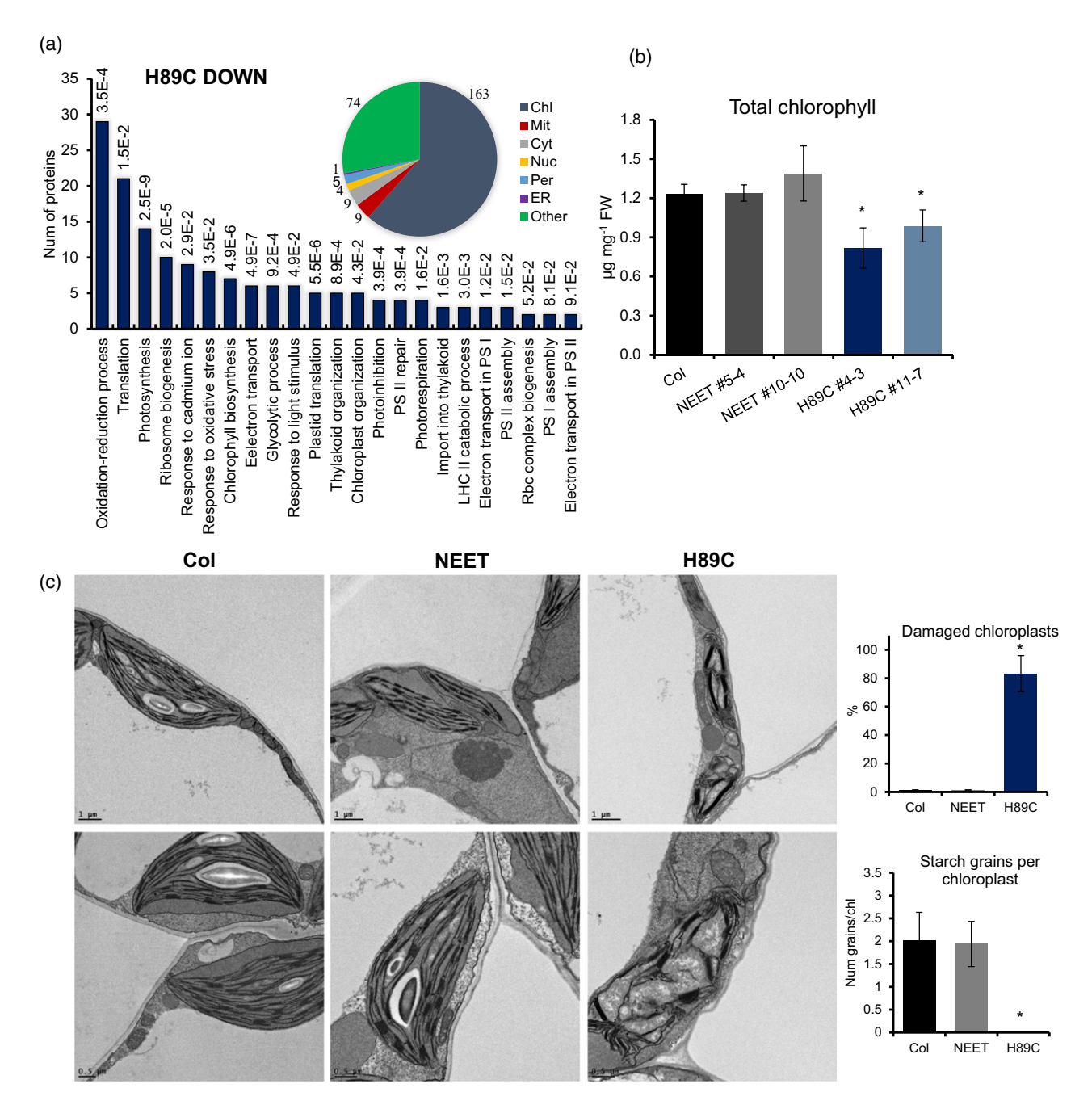


Figure 6. Decrease in the expression of chloroplastic proteins, low chlorophyll content and structural damage to chloroplasts in seedlings expressing H89C. (a) Pie chart of subcellular localization and gene ontology annotation (numbers above each bar represent P values for statistical significance) of proteins with a significant lower abundance in H89C seedlings (P < 0.05; ANOVA). (b) Chlorophyll content in wild type (Col), and AtNEET- and H89C-expressing seedlings. Student's t-test, SD, n = 3, \*P < 0.05. (c) Transmission electron microscope images (left) and quantification bar graphs (right) showing structural damage to chloroplasts in seedlings expressing H89C compared with AtNEET or controls (Col). Student's t-test, SD, n = 250, \*P < 0.05. Scale bar in (c) indicates 1.0 or  $0.2~\mu m$ . NEET, AtNEET-expressing seedlings; H89C, H89C variant of AtNEET-expressing seedlings.

isolated intact chloroplasts from WT, NEET and H89C seedlings, suggested that Fe accumulated in H89C plants in chloroplasts that appeared darker than in WT or NEET plants, and accumulated more Fe (Figure 7c-e). In contrast, Fe did not accumulate in the mitochondria of H89C plants (Figure S5).

#### Cluster transfer from AtNEET to DRE2

The finding that H89C expression altered the expression of cytosolic Fe-S proteins (Figure 5) prompted us to test whether AtNEET can transfer its clusters to DRE2, a key member of the cytosolic Fe-S biogenesis machinery that

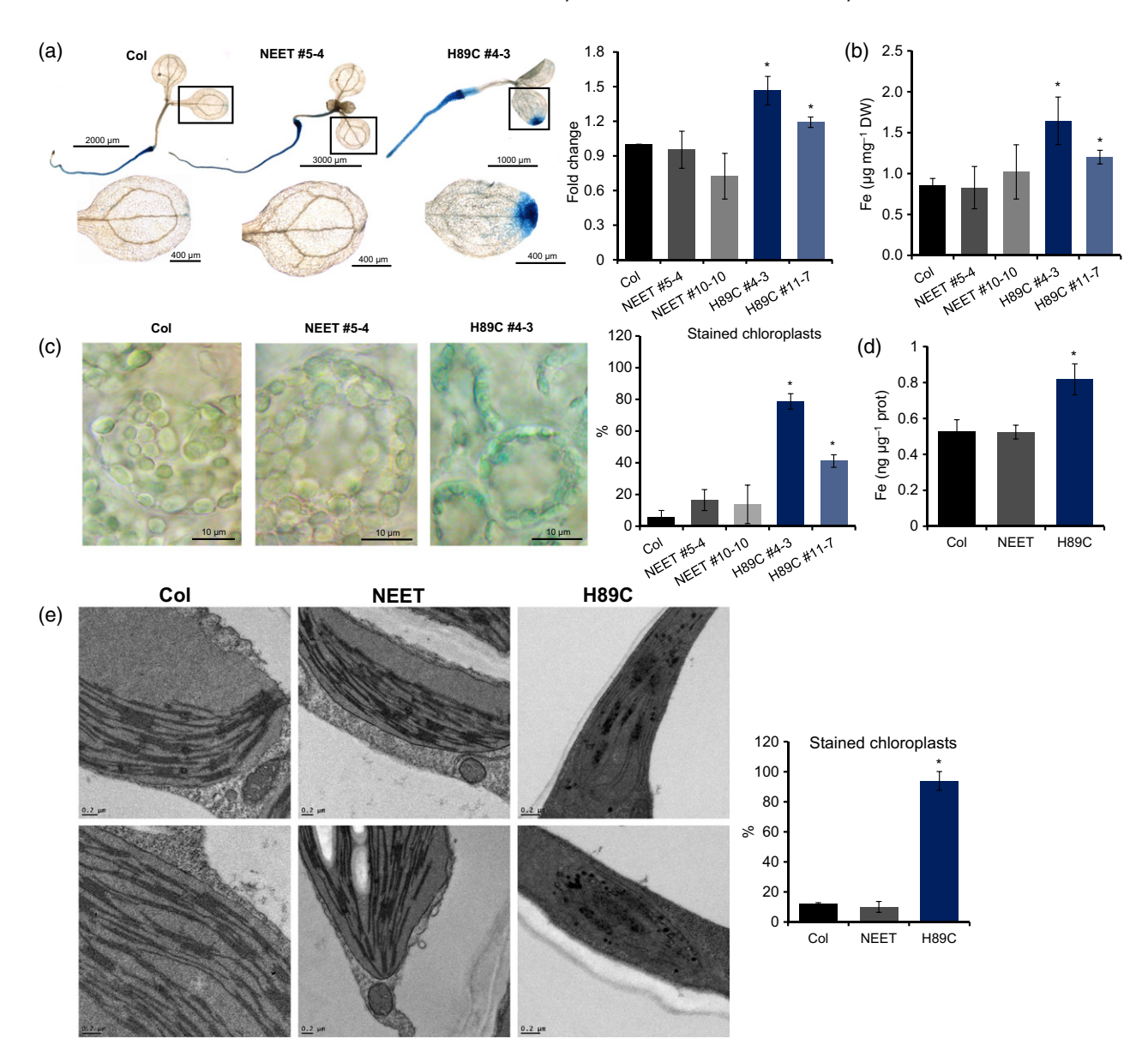


Figure 7. Accumulation of iron in seedlings expressing the H89C variant of AtNEET. (a) Images (left) and bar graph (right) showing Pearl's staining in cotyledons of wild type (WT), NEET and H89C seedlings. Student's t-test, SD, n = 40, \*P < 0.05 (b) Inductively coupled plasma optical emission spectrometry (ICP-OES) measurements of iron in WT, NEET and H89C seedlings. Student's t-test, SD, n = 3, \*P < 0.05 (c) Light microscopy images (left) and a quantification bar graph (right) showing Pearl's staining of chloroplasts from WT, NEET and H89C seedlings. Student's t-test, SD, n = 60, \*P < 0.05. (d) Inductively coupled plasma mass spectroscopy (ICP-MS) measurements of iron in isolated intact chloroplasts from WT, H89C (average of H89C #4-3, #11-7, #23-10) and NEET (average of NEET #5-4, NEET #10-10, NEET #11-9) seedlings. Student's t-test, SD, n = 9, \*P < 0.05. (e) Transmission electron microscopy images (left) and a quantification bar graph (right) showing Pearl's staining of cytosol and chloroplasts in WT, NEET and H89C seedlings. Student's t-test, SD, n = 100, \*P < 0.05. NEET, AtNEET-expressing seedlings; H89C, H89C variant of AtNEET-expressing seedlings.

contains binuclear (2Fe-2S) and tetranuclear (4Fe-4S) Fe-S clusters (Bernard et al., 2013; Lipper et al., 2015). The mammalian NEET proteins NAF-1 and mitoNEET were previously shown to transfer their 2Fe-2S clusters to Anamorsin/ CIAPIN1 (the mammalian homolog of DRE2; Lipper et al., 2015). As shown in Figures 8 and S6, At-NEET, but not H89C, was able to transfer its clusters to DRE2. The ability of AtNEET to transfer its 2Fe-2S cluster to DRE2 was assessed after holo-AtNEET, or holo-H89C, were incubated for increasing lengths of time with apo-DRE2 followed by two analytical methods: native polyacrylamide gel electrophoresis (PAGE) (Figure 8a) and absorption spectroscopy (Figures 8b,c and S6). Because the presence of the Fe-S cluster in AtNEET or DRE2 make these proteins appear as a red band on native gels, we incubated holo-AtNEET, or holo-H89C, with apo-DRE2 for 0 and 60 min, separated them by native PAGE, and followed the 2Fe-2S cluster transfer from holo-AtNEET (upper band, 0 min) to DRE2

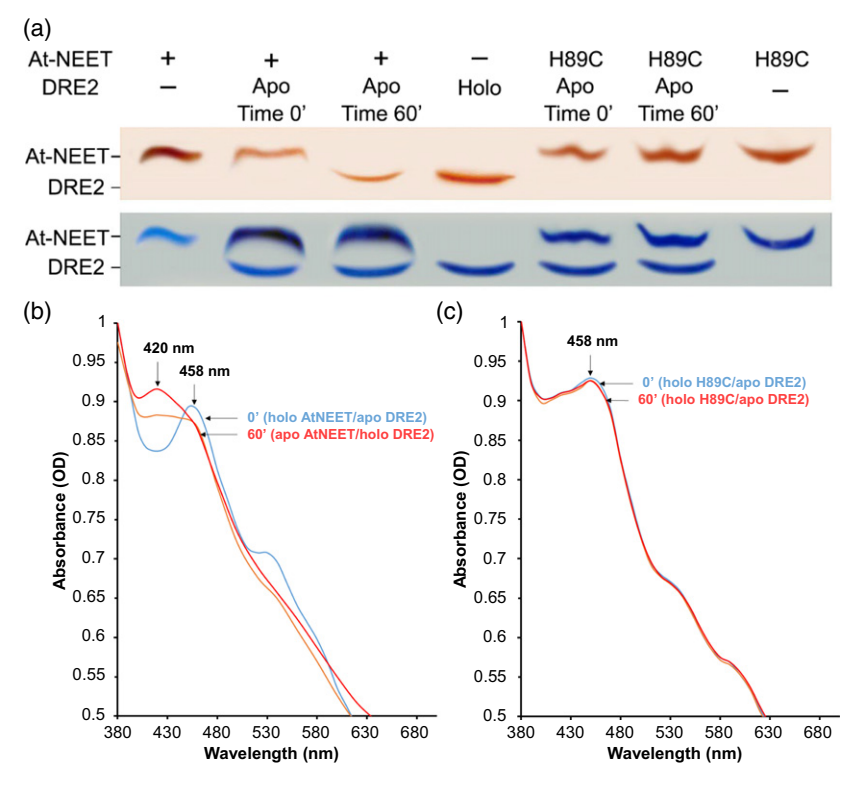


Figure 8. Cluster transfer from AtNEET to DRE2. (a) 2Fe–2S cluster transfer from holo-AtNEET to apo-DRE2 analyzed by native PAGE. The soluble form of holo-AtNEET and pre-reduced apo-DRE2 were incubated for 60 min. The two proteins were then separated by native-PAGE gel, photographed (upper gel), stained with Coomassie blue, and photographed again (lower gel). The upper band corresponds to AtNEET and the lower band corresponds to DRE2. Following 60 min of incubation, the red band representing the holo-form of AtNEET, present at time 0 in the upper gel, disappeared and the red band corresponding to the holo-form of DRE2 appeared. The AtNEET-H89C mutant did not transfer its cluster to apo-DRE2. (b) UV-VIS analysis of 2Fe–2S cluster transfer from holo-AtNEET to apo-DRE2 protein. Soluble AtNEET (holo) and the pre-reduced apo-DRE2 were incubated for 1 h and the absorption spectrum was monitored over time (0 min, blue curve; 30 min, orange curve; and 60 min, red curve). Following the 1-h incubation, the AtNEET characteristic 458-nm absorption peak is lost, whereas the absorption peak corresponding to the holo form of DRE2 (red curve) appears. (c) UV-VIS analysis of cluster transfer reaction from holo-H89C to apo-DRE2 protein. Unlike the cluster transfer observed in (b) between holo-AtNEET and apo-DRE2, no shift in the major absorption peaks is detected when holo-H89C and pre-reduced apo-DRE2 were incubated for 30 min or 1 h. The absorption spectra correspond to holo-H89C/apo-DRE2 (0 min, blue curve; 30 min, orange curve; and 60 min, red curve).

(lower band, 60 min). Visualizing both proteins in the gel, regardless of Fe-S content, was then achieved by Coomassie blue staining. Holo-AtNEET, but not holo-H89C, was shown by this method to transfer its 2Fe-2S clusters to DRE2 (Figure 8a). Because holo-DRE2 was shown to have a peak absorption at 420 nm (Figure 8b, red line; Bernard et al., 2013), whereas holo-AtNEET has a typical peak absorption at 458 nm (Figure 8b, blue line; Nechushtai et al., 2012), it is possible to follow the kinetics of cluster transfer by following changes in absorption spectroscopy between these two peaks (Figures 8b,c and S6). Incubation of holo-AtNEET, or holo-H89C, with apo-DRE2 therefore presented a peak of 458 nm at time 0 (blue line, 0 min), but the absorption of the holo-AtNEET-apo-DRE2 incubation slowly transitioned into a peak at 420 nm at 60 min (red line, 60 min), whereas the incubation of the holo-H89CapoDRE2 did not (Figure 8c). The results presented in Figures 8 and S6 demonstrate that in contrast to holo-AtNEET, holo-H89C is unable to donate its clusters to DRE2.

#### **DISCUSSION**

Although AtNEET was found to be localized to the chloroplast (Nechushtai et al., 2012; Su et al., 2013), and the suppression of its expression was shown to cause impaired growth, early senescence, and the accumulation of Fe and ROS in Arabidopsis plants (Nechushtai et al., 2012), the function of AtNEET in relation to its localization and the phenotypes its suppression induced were unclear. Here we show that disrupting AtNEET function using a dominantnegative strategy (Darash-Yahana et al., 2016) impairs chloroplastic 2Fe-2S metabolism and causes the enhanced expression of many different transcripts involved in Fe-deficiency responses, Fe-S biosynthesis in mitochondria, cytosol and chloroplasts, and Fe-S proteins (Figures 4 and 5). Proteomics analysis shows that despite the higher expression levels of transcripts encoding Fe-S proteins, the abundance of several Fe-S proteins, and in particular 2Fe-2S, in H89C plants is low (e.g. FD1; Figure 5). The apparent discrepancy between the high expression levels of transcripts encoding Fe-S proteins and low abundance of Fe-S proteins, in the presence of sufficient Fe (i.e. not under Fe-deficient conditions), suggests that the disruption in AtNEET function blocked the transfer of Fe-S clusters from the chloroplastic 2Fe-2S biogenesis machinery to chloroplastic (e.g. FD1; Figures 5 and 9) and cytosolic (e.g. DRE2; Figures 8 and 9) 2Fe-2S proteins. The result of such blockage could mediate some of the stunted growth and chlorosis phenotypes (Figures 1 and 2a), especially as FD is suppressed and this protein is essential for chloroplast function and plant growth (Hantzis et al., 2018). The mutation in AtNEET (H89C), which converted the 2Fe-2S cluster binding coordinates of AtNEET from 3Cys-1His to 4Cys, stabilizes the AtNEET cluster >10-fold (Nechushtai et al., 2012), and this fits well with a model in which H89C blocks AtNEET function in mobilizing clusters from the chloroplastic 2Fe-2S biogenesis pathway to target proteins such as FD1 and DRE2 (via a dominant-negative effect; Figures 8 and 9). Indeed, whereas WT AtNEET can donate its cluster to FD or DRE2 in vitro, H89C is unable to do this (Figure 8; Nechushtai et al., 2012). If AtNEET is unable to transfer 2Fe-2S clusters to FD1 or DRE2 it could disrupt photosynthesis and many cytosolic functions, resulting in the formation of ROS and a severe stunted and chlorotic seedling phenotype (Figures 1-3; Table 1; Gao et al., 2013; Rey et al., 2017; Hantzis et al., 2018).

In addition to the chloroplast, AtNEET may also be localized to the mitochondria (Nechushtai et al., 2012). In addition, if AtNEET functions in a similar manner in plant and animal cells (Nechushtai et al., 2012; Tamir et al., 2015; Mittler et al., 2018), in which homodimeric NEET proteins are primarily localized to the outer mitochondrial and/or ER membranes, it might also be localized on the chloroplast and mitochondrial outer membranes. Being localized inside the chloroplast, as well as on its outer membrane (and at the mitochondria) would implicate AtNEET in mediating 2Fe-2S cluster transfer between these different subcellular compartments and the cytosol. Indeed AtNEET, but not H89C, was able to transfer its 2Fe-2S clusters to DRE2, a key cytosolic Fe-S assembly factor (Figure 8). This finding, as well as the elevated expression of DRE2 in H89C (Figure 5), could explain the drastic effect that H89C expression has on the expression of all Fe-S biogenesis pathways in the mitochondria, chloroplast and cytosol, and suggests that AtNEET could also be involved in transferring 2Fe-2S clusters from the chloroplast/mitochondria to the cytosol (Figures 5 and 9). Alternatively, a disruption in chloroplastic Fe-S metabolism may affect all pathways via the activation of a retrograde pathway that senses the level of Fe-S proteins in the chloroplast, and regulates Feand Fe-S-related transcript expression and Fe uptake into the chloroplast (Figures 4, 5, 7 and 9). In this respect it should be noted that AtNEET is primarily expressed in green tissues and leaves, and that expression of H89C appears to have primarily affected the structure of chloroplast and not mitochondria, nuclei or other subcellular compartments (Figure 6). Thus, although plant mitochondria are sensitive to disruptions in Fe-S metabolism (Armas et al., 2019), the role of AtNEET in Fe-S metabolism might be more prominent in the chloroplast compared with the mitochondria.

The disruption in mobilizing 2Fe-2S clusters from the chloroplastic Fe-S biogenesis pathway to target proteins in H89C plants appears to have triggered a leaf-associated Fedeficiency response that involves the PYE network, Fe remobilization from storage compartments (by natural resistance-associated macrophage proteins, NRAMPs) and

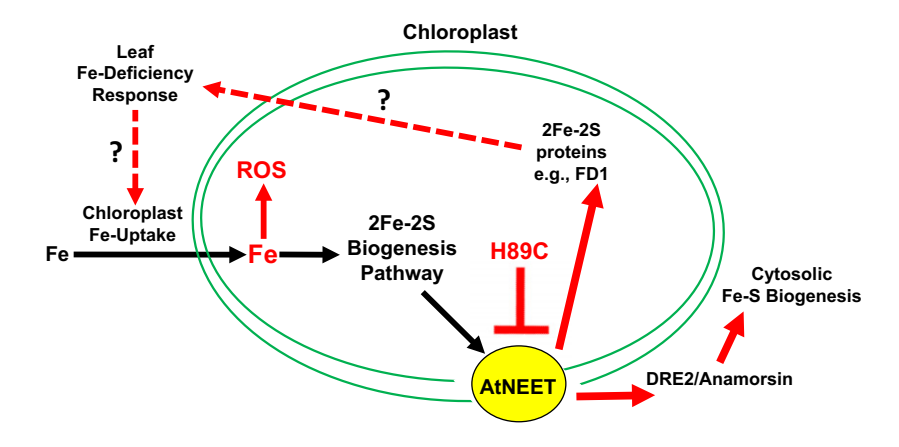


Figure 9. Proposed model for AtNEET function in plants. A hypothetical model showing that AtNEET is required for the mobilization of 2Fe-2S clusters from the chloroplastic Fe-S biogenesis machinery to chloroplastic and cytosolic Fe-S proteins. Blocking the function of AtNEET via expression of the dominant-negative AtNEET variant H89C blocks the mobilization of some 2Fe-2S clusters within and outside of the chloroplast and triggers a partial Fe-deficiency response that results in an over-accumulation of Fe in the chloroplast and enhanced ROS accumulation. Dashed arrows and a question mark indicate a potential retrograde signal, and red fonts and arrows indicate the effects of AtNEET inhibition by H89C expression. H89C, H89C variant of AtNEET; FD1, Ferredoxin 1; Fe, iron; ROS, reactive oxygen species.

uptake into the chloroplast (Figure 4). This transcriptional program is ultimately reflected in the over-accumulation of Fe in the chloroplast (Figure 7c-e). These findings suggest that chloroplastic Fe-S homeostasis, and the abundance of cytosolic and chloroplastic 2Fe-2S proteins (perhaps even AtNEET itself), could function as an indicator for Fe levels in green tissues. The disruption of Fe-S metabolism may therefore trigger an Fe-deficiency response in leaves, even though Fe levels are normal or even elevated (Figure 7a,b). The triggered Fe-deficiency response may cause the accumulation of Fe in chloroplasts (Figure 7c-e), but this Fe is not used for the production of Fe-S proteins (Figure 5c) and could result in the enhanced accumulation of ROS and damage to chloroplasts (Figures 3, 6 and 9; Duy et al., 2011). Interestingly, this response appears to be specific for 2Fe-2S metabolism and was not associated with elevated levels of several heme proteins (Figure 5c). Because direct H<sub>2</sub>O<sub>2</sub> application to seedlings (albeit for 8 min with no apparent visible phenotype, as opposed to the contentious expression of H89C in seedlings for 7 days that resulted in a visible phenotype; Zandalinas et al., 2019) did not result in Fe- and Fe-S-transcriptomic signatures, similar to those reported here for H89C expression (Figures 4 and 5), it is likely that the disruption in Fe and Fe-S metabolism induced by H89C expression (Figure 7) triggered ROS accumulation and ROS-associated transcriptomic signatures (Figure 3). H89C expression therefore altered Fe and Fe-S metabolism that in turn caused enhanced ROS levels (Figure 9). This finding highlights the intimate link between Fe/Fe-S and ROS in cells (e.g. Lill, 2009; Boyd et al., 2014; Andreini et al., 2017), and suggests that AtNEET function needs to be tightly regulated in order to prevent Fe, Fe-S and ROS imbalances, such as those observed in H89C plants.

Interestingly, the Fe-deficiency response activated in H89C plants (i.e. the PYE network, NRAMPs and mitochondrial/chloroplast Fe uptake) appears to be specific to leaves (local) without being systemically propagated to roots (Thomine and Vert, 2013; Brumbarova et al., 2015; Le et al., 2016; Jeong et al., 2017; Khan et al., 2018; Kobayashi et al., 2019). For instance, although BTS, ILR3 and PYE are upregulated, FIT and several Fe-responsive root-specific transcripts such as the root Fe2+ uptake transporter (IRT1) and the Fe<sup>3+/2+</sup> reductase (FRO2) are not. This observation could be explained by the presence of high levels of labile Fe and ROS in H89C plants (Figure 7a,b). The Fe that is present in forms other than Fe-S clusters in H89C plants could be loaded into the phloem and complete the shoot-to-root signaling route, thus preventing FIT induction. Moreover, it has been previously shown that Zat12, which is highly induced in H89C plants, is also induced by ROS and may block the function of FIT, thus repressing a possible Fe-deficiency response in roots (Le et al., 2016). Taken together, it appears that the PYE network and other Fe-responsive

transcripts specific to leaves are induced when the metabolism of 2Fe–2S clusters is impaired in chloroplasts, even in the presence of high levels of Fe in leaves. The Fe-deficiency response observed in H89C plants was not propagated systemically to roots, however, probably because of the presence of high ROS levels, which are capable of blocking the FIT network in roots in a Zat12-dependent manner.

The activation of a partial Fe-deficiency response in H89C (Figure 4), coupled with the blockage or disruption in the biosynthesis of 2Fe–2S proteins (Figure 5), could potentially result in a vicious cycle of events that overloads the chloroplast with Fe (a consequence of the Fe-deficiency response; Figures 4 and 9). This Fe is not used for Fe–S cluster biogenesis (a consequence of the H89C mutation; Figure 5) and its accumulation results in enhanced ROS levels (Figure 3; Table 1) and chloroplast destruction (Figure 6). This cycle of events could be similar to what happens in the mitochondria of patients with Friedreich's ataxia caused by a disruption in Frataxin (Mena *et al.*, 2015), a protein involved in Fe mobilization and Fe–S biogenesis in the mitochondria.

The link identified in this work between 2Fe–2S metabolism in the chloroplast and cytosol and the induction of a leaf Fe-deficiency response could suggest that part of the way Fe is sensed in plants is tightly linked to 2Fe–2S cluster metabolism, and/or the abundance of a particular 2Fe–2S protein(s). Moreover, this Fe deficiency response could be mediated from the chloroplast via a retrograde signal, or by the transfer of 2Fe–2S clusters from the chloroplast to the cytosol (via DRE2; Figure 8). Because leaves play a major role in regulating Fe uptake by roots (Khan *et al.*, 2018), the chloroplast and Fe–S metabolism that occurs in leaves may have a more profound effect on Fe sensing than previously thought. Further studies are of course needed to address this possibility.

## **EXPERIMENTAL PROCEDURES**

#### Plant material

AtNEET (At5G51720) was amplified by polymerase chain reaction (PCR) and the H89C sequence was generated by site-directed mutagenesis, as previously described (Nechushtai et al., 2012). Both sequences were cloned into a pGREEN binary expression vector using Xhol and Sacl sites, downstream of the CaMV 35S promoter. Agrobacterium tumefaciens strain GV3101 (pMP90) was transformed with both constructs and used to obtain NEETand H89C-overexpressing lines (p35S::NEET and p35S::H89C, respectively, from Arabidopsis thaliana Columbia-0) using the floral-dip procedure (Zhang et al., 2006). Transformed lines were selected using hygromycin resistance and AtNEET expression was determined by quantitative real-time PCR (qRT-PCR) and protein blots (using AtNEET antibodies; Nechushtai et al., 2012), as described in Suzuki et al. (2013). CRISPR NEET plants were generating using a pCAMBIA-based vector (pHSE401), according to the method described by Xing et al. (2014). gRNA guide

(5-CATCGCAAGCACGTTCGGCA-3) was designed in https://zlab.b io/guide-design-resources. Detection and null mutation homozygote screening of the target gene modification was performed using hygromycin selection and the Surveyor® Mutation Detection Kit (IDT Cat#706020; Integrated DNA Technologies, https:// www.idtdna.com/pages/products/reagents-and-kits/mutationdetection/surveyor-mutation-detection-kits).

#### **Growth conditions**

Col plants, homozygous NEET-overexpressing lines and homozygous H89C overexpressing lines were grown in peat pellets (Jiffy-7; Jiffy, http://jiffygroup.com) under controlled conditions of 23°C and constant light (50 µmol m<sup>-2</sup> sec<sup>-1</sup>) and monitored for survival, rosette diameter and inflorescence height. For transcriptomics and proteomics analyses, chlorophyll and Fe measurements, and light and TEM microscopy imaging, seeds of Col, two H89C homozygous lines (H89C #4-3 and H89C #11-7; highest expressing surviving plants) and NEET homozygous lines (NEET #5-4 and NEET #10-10; similar or higher expression level to the H89C lines), each with between three and five technical repeats, were surface-sterilized with bleach and placed on 1% agar plates (half-strength MS medium). Seedlings were grown at 23°C under constant light (50 µmol m<sup>-2</sup> sec<sup>-1</sup>) for 7 days and about 80-100 seedlings from each technical repeat were frozen in liquid nitrogen or fixed and used for subsequent analyses. For ICP analyses, about 100 sterilized seedlings of each line were grown in 100 ml of sterile half-strength MS on a shaker (150 rpm) under constant light (50 µmol m<sup>-2</sup> sec<sup>-1</sup>) for 7 days, as described in Zandalinas et al. (2019).

#### RNA sequencing and differential gene expression analysis

Total RNA from about 80-100 seedlings of each line (Col, NEET #5-4, NEET #10-10, H89C #4-3 and H89C #11-7) was isolated using TRIzol (Invitrogen, now ThermoFisher Scientific, https://www.ther mofisher.com/us/en/home/brands/invitrogen) and purified using a NucleoSpin RNA Clean-up kit (Macherey-Nagel, https://www.mnnet.com/). Initial RNA sample quality was assessed with a Bioanalyzer RNA 6000 Nano Kit (Agilent, https://www.agilent.com) using the 2100 Bioanalyzer System (Agilent) and RNA quantification was assessed with a Qubit RNA Broad Range Assay Kit (Invitrogen) using the Qubit 3.0 Fluorometer (Invitrogen). RNA libraries were prepared from 1 µg of total RNA and dual-indexed with a TruSeq Stranded mRNA HT Library Prep Kit (Illumina, https://www.illu mina.com). The resulting cDNA libraries were quantified with a Qubit dsDNA High Sensitivity Assay Kit (Invitrogen) on a Qubit 3.0 Fluorometer (Invitrogen). Fragment length was validated on a 4200 TapeStation System (Agilent) with a TapeStation D1000 Assay Kit (Agilent), prior to library pooling and normalization to a loading concentration of 1.6 pm. Sequencing was performed as previously described (Zandalinas et al., 2019) using four NextSeq High Output 1 x 75 Reagent Cartridges (Illumina) on a NextSeq 500 Sequencing Platform (Illumina), and produced 1.81 G (PF) reads with  $Q \ge 93.84\%$ . RNA library construction and sequencing were performed by the BioDiscovery Institute Genomics Center at the University of North Texas (http://bdi.unt.edu/genomics-center). Single-end sequenced reads were quality tested using FASTOC 0.11.7 (Andrews, 2010) and aligned to the reference genome of Arabidopsis (genome build 10) obtained from TAIR (https://www.arabidopsis.org) using STAR ALIGNER 2.4.0.1 (Dobin et al., 2013). Default mapping parameters (10 mismatches per read and nine multimapping locations per read) were used. The genome index was generated using the gene annotation file (gff file) obtained from TAIR for genome build 10. Raw and processed RNA-Seq data files were deposited in GEO (https://www.ncbi.nlm. nih.gov/geo/) under the following accession number: GSE127300. Differential gene expression analysis was carried out using DESEo2 1.20.0, an R-based package available from Bioconductor (https://www.bioconductor.org) (Love et al., 2014). Differentially expressed transcripts were identified by examining the difference in their abundance, measured as the mean normalized count of reads mapping onto the transcript (Love et al., 2014). The difference in expression was quantified in terms of the logarithm of the ratio of mean normalized counts between two conditions (log fold change). Gene ontology enrichment and annotations (GO biological process, P < 0.05) of differentially expressed transcripts were performed using DAVID Bioinformatics Resources 6.8 (https://da vid.ncifcrf.gov/home.jsp; Huang et al., 2009). Enrichment in hormone (ABA, ACC, brassinolide, cytokinin, gibberellin, indole-3-acetic acid, methyl jasmonate and salicylic acid) or ROS (H<sub>2</sub>O<sub>2</sub>, O<sub>2</sub> and <sub>1</sub>O<sup>2</sup>) response transcripts was calculated as described by Zandalinas et al. (2019).

#### Proteomic analysis

Seven-day-old Arabidopsis seedlings (80-100; Col, NEET #5-4, NEET #10-10, H89C #4-3 and H89C #11-9) grown on 1% agar halfstrength MS plates, as described above, were used for proteomic analyses. Samples were processed as described by Dahal et al. (2016). An aliquot of each protein sample was centrifuged and protein pellets were then re-suspended with 75  $\mu I$  of 6 M urea, 2 Mthiourea and 100 mm ammonium bicarbonate. Samples were subjected to an EZQ quantitation using MULTI GAUGE 2.3. trypsin digestion, 25  $\mu g$  of proteins from each sample were reduced and alkylated, digested with trypsin (ratio 1:50 trypsin:protein, w/w), and peptides were purified by Pierce C18 tips. Purified peptides were then lyophilized and resuspended in 5/0.1% acetonitrile/formic acid. For liquid chromatography with tandem mass spectrometry (LC-MS/MS) analyses (timsTOF pro; Bruker, https://www. bruker.com/products/mass-spectrometry-and-separations/lc-ms/otof/timstof-pro.html), 0.8 µg suspended peptide was separated on a C18 column (20 cm  $\times$  75  $\mu$ m, 1.7  $\mu$ m) with a step gradient of acetonitrile at 300 ml  $\mathrm{min}^{-1}$ . The Bruker nanoElute system (Bruker, https://www.bruker.com) was connected to a timsTOF pro mass spectrometer and the LC gradient conditions were established as follows: initial conditions were 2% B (A, 0.1% formic acid in water; B, 99.9% acetonitrile, 0.1% formic acid), followed by 20 min ramp to 17% B; 17-25% B over 27 min, 25-37% B over 11 min, gradient of 37% B to 80% B over 6 min and hold at 80% B for 6 min. The total run time was 70 min. MS data were collected over an m/z range of 100-1700. During MS/MS data collection, each tims cycle included one MS plus an average of 15 parallel accumulation-serial fragmentation (PASEF) MS/MS scans. The acquired data were submitted to the PEAKs search engine for protein identification. The TAIR 10 protein database was used. Data were searched with trypsin as the enzyme, and with two missed cleavages allowed, carbamidomethyl cysteine as a fixed modification, oxidized methionine and deamidation of asparagine and glutamine as variable mod, 50 ppm mass tolerance on precursor ions and 0.1 Da on fragment ions. For quantitative analysis, protein FASTA sequences for 12 proteins (PetC, PAO, CAO, TIC55, FDC1, Glu1, Glu2, PsaA, PsaB, Nir1, SiR and SiRB) were imported into SKYLINE to identify a set of between three and six unique peptides for each protein based on the TAIR 10 proteome. Areas for each peptide signal (or summed areas of multiple peptides) were normalized using the prominent trypsin autolysis peptide (108 VATVSLPR115). Peptide digests resuspended in 25 μl of 5% acetonitrile and 1% formic acid (at 1  $\mu$ g  $\mu$ l<sup>-1</sup>) were separated using a gradient method (50 min). A full-loop injection (10 µl) was loaded

onto a C8 trap column (pepmap100; ThermoFisher Scientific, https://www.thermofisher.com). Peptides were eluted from the trap column and separated on a 20 cm × 75 μm inner diameter pulled-needle analytical column packed with HxSIL C18 reversedphase resin (Hamilton Co., https://www.hamiltoncompany.com) with a step gradient of acetonitrile at 500 nl min<sup>-1</sup>. The Eksigent Nano 1D plus HPLC system was attached to a Thermo Scientific TSQ Quantiva triple-quadrupole mass spectrometer. Initial LC gradient conditions were 2% B (A, 0.1% formic acid in water; B, 99.9% acetonitrile; 0.1% formic acid), followed by 2 min ramp to 10% B, gradient 10-40% B over 36 min, ramp to 90% B in 1 min, hold at 90% B for 7 min, ramp back to (1 min) and hold at (5 min) initial conditions. The total run time was 50 min. Multiple reaction monitoring (MRM) conditions were: ionization voltage 1600 V, Q1 resolution 1.2, Q3 resolution 0.7 (full-width half-max), collision gas 3 mTorr. Data for between one and six peptides were acquired for each protein. Following acquisition, the most prominent peptides (and transitions per peptide) were examined and a subset of peptides/transitions was used for quantitation. Ratios of proteins of interest versus trypsin autolysis peptide were calculated. Student's t-tests were conducted on the triplicates in each group (pairwise comparisons) and those with a P < 0.05 were identified. All proteomic analyses were performed by the Gehrke Proteomics Center at the University of Missouri (http://proteomics.missouri.edu). Proteomics data were deposited in the Proteome Xchange (https://panoramaweb.org/Mittler-FeS-prots.url; PX ID PXD015447, http://proteomecentral.proteomexchange.org/cgi/GetDataset?ID= PXD015447).

# Chlorophyll measurements

Chlorophyll extraction was performed as described by Moran (1982), with some modifications. About 50–70 mg of 7-day-old seedlings of each line were incubated in 5 ml of *N,N*-dimethylformamide (DMF) at 4°C in the dark for 7 days. Then, the absorbance of 1 ml of the DMF extraction was read in a spectrophotometer at 603, 647 and 664 nm, using 1 ml of clean DMF as blank.

#### Pearl's staining of ferric iron in seedlings

The Pearl's staining method was adapted from Schuler et al., (2012) and Armas et al., (2019). Briefly, fresh 7-day-old seedlings of each line growing on 1% agar half-strength MS supplemented with 0.35 mm FeSO<sub>4</sub>7H<sub>2</sub>O were vacuum infiltrated for 1 h at room temperature (21-23°C) with fixative solution (methanol/chloroform/acetic acid, 6:3:1). The fixative was removed and seedlings were washed three times with distilled water and subsequently vacuum infiltrated with equal volumes of Pearl's stain solution (4% HCl and 4% K-ferrocyanide, 1:1) for 1 h at room temperature. The reaction was stopped by washing three times with distilled water. Seedlings were visualized and imaged under the microscope and the blue color intensity was measured by using blue histograms with IMAGEJ 6 (https://imagej.nih.gov). The measurement of Pearl's levels and counting organelles with a high level of Pearl's stain in light or electron microscopy was conducted as described previously (Zumbrennen-Bullough et al., 2014; Grishchuk et al., 2015; Leclerc et al., 2015; Ahmad et al., 2017; Khalaf et al., 2019).

# Inductively coupled plasma optical emission spectrometry (ICP-OES)

About 100 seedlings of each line grown in half-strength MS as describe above were rinsed in deionized water for 10 min, washed in 20 mm Tris-HCl (pH = 8) containing 5 mm EDTA on a shaker for

10 min, and then washed in deionized water on a shaker for an additional 10 min. Seedlings were dried at 60°C for 3 days and the dry weight was recorded. The tissues were digested in trace metal-grade nitric acid for 3 days and, to ensure complete digestion, samples were boiled for 15 min three times. The digested samples were diluted 1:10 with milliQ water and extracts were analyzed for Fe concentration using an ICP-OES (Optima 8000; PerkinElmer, https://www.perkinelmer.com/category/inductively-coupled-plasma-icp-oes). Three different biological repeats of each line were analyzed.

#### Inductively coupled plasma mass spectrometry (ICP-MS)

About 100 seedlings of each line grown in half-strength MS as describe above were rinsed in deionized water for 10 min, washed in 20 mm Tris-HCI (pH = 8) containing 5 mm EDTA on a shaker for 10 min, and then washed in deionized water on a shaker for an additional 10 min. Intact chloroplasts for each line were purified by using  $\mathsf{Minute}^{\scriptscriptstyle\mathsf{TM}}$  Chloroplast Isolation Kit (Invest Biotechnologies, https://inventbiotech.com) following the manufacturer's instructions, and protein concentration was calculated according to Bradford, (1976) using bovine serum albumin as a standard. Chloroplasts were diluted in 300 µl of concentrated HNO3 (Fisher Optima grade). The acid mixture was heated in a hot block at 75°C for 2 h. After digestion, samples were made up to 10 ml with ultrapure water. A solution of internal standards, Sc, Y, In and TI, was weighed into each. Two digestion blanks were prepared in the same way alongside the samples. Analysis of these blanks did not reveal any significant background level of the elements of interest. Samples were analyzed on a PerkinElmer NexION 300X with a glass nebulizer and glass cyclonic spray chamber. The Nex-ION was operated in Kinetic Energy Discrimination (KED) mode, which uses a collision cell to diminish the prevalence of polyatomic interferences. Fe was measured in two different KED cell gas flow groups: 2.5 and 4.5 ml He min<sup>-1</sup>. The NexION was calibrated using a series of multielement standards prepared from a commercial High Purity Standards stock solution. Internal standards Sc, Y, In, and TI were added to instrument blanks and all linearity standards. Instrument limits of detection were calculated as three times the standard deviation of the concentration measured in 10 analyses of zero-point standard (blank 3% HNO3 solution with internal standards). Sample limits of detection were the instrument limit of detection multiplied by the exact gravimetric dilution factor for each sample. Three different biological repeats of each line (H89C #4-3, #11-7, #23-10 and NEET #5-4, NEET #10-10, NEET #11-9; Figure 1) were analyzed and the average of the three NEET lines and the three H89C lines was calculated.

#### Transmission electron microscopy

Seedlings were fixed in 2% paraformaldehyde and 2% glutaraldehyde in 100 mm sodium cacodylate buffer, pH 7.35. For Pearl's staining, fixed tissues were rinsed with 100 mm sodium cacodylate buffer, pH 7.35, containing 130 mm sucrose and immersed in 0.25% Pearl's staining solution for 1 h at 4°C, followed by three cacodylate buffer rinses. Secondary fixation was performed using 1% osmium tetroxide (Ted Pella, Inc., https://www.tedpella.com) in cacodylate buffer using a Pelco Biowave (Ted Pella, Inc.) operated at 100 W for 1 min. Seedlings were next incubated at 4°C for 1 h, then rinsed with cacodylate buffer and further with distilled water. En bloc staining was performed using 1% aqueous uranyl acetate, incubated at 4°C overnight and then rinsed with distilled water. A graded dehydration series was performed using ethanol, transitioned into acetone, and dehydrated tissues were then infiltrated with a 1v/1v of Epon and Spurr resin for 24 h at room

temperature and polymerized at 60°C overnight. Sections were cut to a thickness of 80 nm using an ultramicrotome (Ultracut UCT; Leica Microsystems; https://www.leica-microsystems.com) and a diamond knife (Diatome, https://www.diatomeknives.com). Images were acquired with a JEOL JEM 1400 transmission electron microscope (JEOL, https://www.jeol.co.jp) at 80 kV on a Gatan Ultrascan 1000 CCD (Gatan, Inc., http://www.gatan.com).

## Protein expression, purification and 2Fe-2S cluster transfer assays

AtNEET and H89C proteins were expressed and purified as described by Nechushtai et al. (2012). Briefly, BL-21 competent Escherichia coli cells were transformed with a pET28-a (+) vector containing the cDNA of the soluble form of AtNEET/H89C and grown in LB supplemented with 30 μg ml<sup>-1</sup> kanamycin at 37°C. At an OD600nm of 0.6, 0.75 mm FeCl3 was added and cell growth proceeded for an additional 12 h. After pelleting and lysis, AtNEET/ H89C proteins were purified using an Ni-NTA column followed by size-exclusion chromatography, as described by Nechushtai et al. (2012). The cDNA of the His-Tag-DRE2 (At5g18400) protein, was cloned into pET28-a (+) vector (Novagen, now Merck, http://www. merckmillipore.com) and transformed in E. coli (BL-21). Transformed cells were grown in LB media, supplemented with  $30~\mu g~m l^{-1}$  kanamycin at  $37^{\circ} C.$  At an  $OD_{600nm}$  of 0.6, 0.75 mm FeCl<sub>3</sub> with isopropyl  $\beta$ -D-1-thiogalactopyranoside (IPTG) (0.2 mg ml<sup>-1</sup>) was added and cell growth proceeded for an additional 4 h. Cells were then harvested and homogenized in 25 mm Tri-HCl, pH 8.0, and 250 mm NaCl with 5 mm imidazole. Following lysis and centrifugation the supernatant was bound to a nickel-NTA column, eluted and purified by size-exclusion chromatography, as described by Nechushtai et al. (2012). The holo form of DRE2 was then concentrated using a 10-kD centricon (Amicon®; Sigma-Aldrich, https://www.sigmaaldrich.com/technical-docume nts/articles/biology/amicon-ultra-centrifugal-filters.html), into 500 mm dithiothreitol (DTT), 200 mm Na2-ethylenediaminetetraacetic acid (EDTA), pH 8.0 (to a final concentration of 4 mg ml<sup>-1</sup>) and heated for 8 min at 52°C until the protein becomes colorless. Apo-DRE2 was then dialyzed against a buffer containing 25 mm Tris-HCl, pH 8.0, 250 mm NaCl and 2.5 mm DTT. 2Fe-2S cluster transfer assays were performed as follows: Apo-DRE2 (250  $\mu\text{M}$ ) was pre-reduced in the presence of 5 mm Nadithionite and 5 mm Na<sub>2</sub>-EDTA, pH 8.0, for 60 min. Apo-DRE2 was then incubated with AtNEET (WT or the H89C mutant; 250 µM), and 2Fe-2S cluster transfer was analyzed by absorption spectroscopy and native-PAGE, as described by Nechushtai et al. (2012) and Lipper et al. (2015). The native-gel conditions were as follows. Staking gel: 4% acrylamide, 250 mm amino caproic acid, 25 mm BIS-TRIS, pH 7.0. Separating gel: 10% acrylamide, 8% glycerol, 250 mm amino caproic acid, 25 mm BIS-TRIS, pH 7.0. The cathode buffer was composed of 50 mm Tricine, 9 mm BIS-TRIS, pH 7.0, and the anode buffer contained 50 mm of BIS-TRIS at pH 7.0.

#### Statistical analysis

Statistical analyses were performed by two-tailed Student's ttest. Results are presented as means  $\pm$  SDs (asterisks denote statistical significance at P < 0.05 with respect to WT, Col). Differentially expressed transcripts or proteins were defined as those that had a fold change with an adjusted P < 0.05 (analysis of variance, ANOVA, and/or negative binomial Wald test followed by a Benjamini-Hochberg correction). Venn diagram overlaps were subjected to hypergeometric testing using PHYPER (R package).

#### **Data statement**

All data referred to in the article and included in the supporting information are deposited in GEO (https://www.ncbi.nlm.nih. gov/geo/) under accession number GSE127300, and in Proteome Xchange (http://proteomecentral.proteomexchange.org/cgi/GetDa taset) under PX ID PXD015447.

#### **ACKNOWLEDGEMENTS**

This work was supported by funding from the National Science Foundation (NSF-BSF MCB-1936590, IOS-1932639 and IOS-1353886 to R.M.; BSF 2015831 to R.N.; and MCB-1818312 to D.G.M.C.), the Bond Life Sciences Early Concept Grant (D.G.M.C. and R.M.), and the University of Missouri. We apologize to all authors of papers not mentioned in this article because of limited

#### **AUTHOR CONTRIBUTIONS**

SIZ, LS, SM, DGG, HBM and NACG performed experiments and analyzed the data. SIZ, SS, DB and RKA conducted bioinformatics and statistical analyses. SIZ, RN, DGMC and RKA designed experiments and analyzed the data. RM, SIZ, DGMC, RN and RKA wrote the article.

#### CONFLICT OF INTEREST

The authors declare no conflicts of interest.

#### SUPPORTING INFORMATION

Additional Supporting Information may be found in the online version of this article.

Appendix S1. List of abbreviations and references used in Figures 3-5.

Figure S1. CRISPR-Cas9 mutation in AtNEET does not abolish AtNEET protein expression.

Figure S2. PCA plot for RNA-Seq data obtained from wild type (Col), AtNEET-overexpressing lines (NEET) and H89C overexpressing lines (H89C).

Figure S3. Gene ontology annotation of transcripts significantly downregulated in AtNEET or H89C plants (numbers above each bar represent P value for statistical significance).

Figure S4. Pie chart of subcellular localization and gene ontology annotation (numbers above each bar represent P value for statistical significance) of proteins with a significantly higher or lower abundance in H89C and NEET seedlings.

Figure S5. Transmission electron microscopy images (top) and a quantification bar graph (bottom) showing Pearl's staining of mitochondria in WT, NEET and H89C seedlings.

Figure S6. UV-VIS analysis of 2Fe-2S cluster transfer from AtNEET to apo-DRE2 protein.

Table S1. Transcripts significantly upregulated in NEET-overexpressing plants compared with WT plants.

Table S2. Transcripts significantly downregulated in NEET-overexpressing plants compared with WT plants.

Table S3. Transcripts significantly upregulated in H89C-overexpressing plants compared with WT plants.

Table S4. Transcripts significantly downregulated in H89C-overexpressing plants compared with WT plants.

Table S5. Proteins significantly upregulated in NEET-overexpressing plants compared with WT plants.

Table S6. Proteins significantly downregulated in NEET-overexpressing plants compared with WT plants.

Table S8. Proteins significantly downregulated in H89C-overexpressing plants compared with WT plants.

#### **REFERENCES**

- Ahmad, A.S., Mendes, M., Hernandez, D. and Doré, S. (2017) Efficacy of laropiprant in minimizing brain injury following experimental intracerebral hemorrhage. Sci. Rep. 7, 9489.
- Andreini, C., Rosato, A. and Banci, L. (2017) The relationship between environmental dioxygen and iron-sulfur proteins explored at the genome level. *PLoS One*, 12, e0171279.
- Andrews, S. (2010) FastQC: a quality control tool for high throughput sequence data. Available at: http://www.bioinformatics.babraham.ac.uk/ projects/fastqc/.
- Armas, A.M., Balparda, M., Turowski, V.R., Busi, M.V., Pagani, M.A. and Gomez-Casati, D.F. (2019) Altered levels of mitochondrial NFS1 affect cellular Fe and S contents in plants. *Plant Cell, Rep.* 38, 981–990.
- Balk, J. and Pilon, M. (2011) Ancient and essential: the assembly of iron-sulfur clusters in plants. *Trends Plant Sci.* 16, 218–226.
- Balk, J. and Schaedler, T.A. (2014) Iron cofactor assembly in plants. Annu. Rev. Plant Biol. 65, 125–153.
- Bernard, D.G., Netz, D.J.A., Lagny, T.J., Pierik, A.J. and Balk, J. (2013) Requirements of the cytosolic iron-sulfur cluster assembly pathway in Arabidopsis. *Philos. Trans. R. Soc. Lond. B Biol. Sci.* **368**, 20120259.
- Boyd, E.S., Thomas, K.M., Dai, Y., Boyd, J.M. and Outten, F.W. (2014) Interplay between oxygen and Fe–S cluster biogenesis: insights from the Suf pathway. *Biochemistry*, 53, 5834–5847.
- Bradford, M.M. (1976) A rapid and sensitive method for the quantitation of microgram quantities of protein utilizing the principle of protein-dye binding. Anal. Biochem. 72, 248–254.
- Brumbarova, T., Bauer, P. and Ivanov, R. (2015) Molecular mechanisms governing Arabidopsis iron uptake. Trends Plant Sci. 20, 124–133.
- Dahal, D., Newton, K.J. and Mooney, B.P. (2016) Quantitative proteomics of Zea mays hybrids exhibiting different levels of heterosis. J. Proteome Res. 15, 2445–2454.
- Darash-Yahana, M., Pozniak, Y., Lu, M. et al. (2016) Breast cancer tumorigenicity is dependent on high expression levels of NAF-1 and the lability of its Fe-S clusters. Proc. Natl. Acad. Sci. USA. 113, 10890–10895.
- Davletova, S., Schlauch, K., Coutu, J. and Mittler, R. (2005) The zinc-finger Protein Zat12 plays a central role in reactive oxygen and abiotic stress signaling in Arabidopsis. *Plant Physiol.* 139, 847–856.
- Dobin, A., Davis, C.A., Schlesinger, F., Drenkow, J., Zaleski, C., Jha, S., Batut, P., Chaisson, M. and Gingeras, T.R. (2013) STAR: ultrafast universal RNA-seg aligner. *Bioinformatics*. 29, 15–21.
- Duy, D., Stube, R., Wanner, G. and Philippar, K. (2011) The chloroplast permease PIC1 regulates plant growth and development by directing homeostasis and transport of iron. *Plant Physiol.* 155, 1709–1722.
- Gao, H., Subramanian, S., Couturier, J. et al. (2013) Arabidopsis thaliana Nfu2 accommodates [2Fe–2S] or [4Fe–4S] clusters and is competent for in vitro maturation of chloroplast [2Fe–2S] and [4Fe–4S] cluster-containing proteins. Biochemistry, 52, 6633–6645.
- Gapinske, M., Luu, A., Winter, J., Woods, W.S., Kostan, K.A., Shiva, N., Song, J.S. and Perez-Pinera, P. (2018) CRISPR-SKIP: programmable gene splicing with single base editors. *Genome Biol.* 19, 107.
- Grishchuk, Y., Pena, K.A., Coblentz, J., King, V.E., Humphrey, D.M., Wang, S.L., Kiselyov, K.I. and Slaugenhaupt, S.A. (2015) Impaired myelination and reduced brain ferric iron in the mouse model of mucolipidosis IV. *Dis. Model. Mech.* 8, 1591–1601.
- Hantzis, L.J., Kroh, G.E., Jahn, C.E., Cantrell, M., Peers, G., Pilon, M. and Ravet, K. (2018) A program for iron economy during deficiency targets specific Fe proteins. *Plant Physiol.* 176, 596–610.
- Hindt, M.N., Akmakjian, G.Z., Pivarski, K.L., Punshon, T., Baxter, I., Salt, D.E. and Guerinot, M.Lou (2017) BRUTUS and its paralogs, BTS LIKE1 and BTS LIKE2, encode important negative regulators of the iron deficiency response in Arabidopsis thaliana. *Metallomics*, 9, 876–890.
- Hu, X., Kato, Y., Sumida, A., Tanaka, A. and Tanaka, R. (2017) The SUFBC 2 D complex is required for the biogenesis of all major classes of plastid Fe-S proteins. *Plant J.* 90, 235–248.

- Huang, D.W., Sherman, B.T. and Lempicki, R.A. (2009) Systematic and integrative analysis of large gene lists using DAVID bioinformatics resources. Nat. Protoc. 4, 44–57.
- Jeong, J., Merkovich, A., Clyne, M. and Connolly, E.L. (2017) Directing iron transport in dicots: regulation of iron acquisition and translocation. *Curr. Opin. Plant Biol.* 39, 106–113.
- Khalaf, S., Ahmad, A.S., Chamara, K.V.D.R. and Doré, S. (2019) Unique properties associated with the brain penetrant iron chelator HBED reveal remarkable beneficial effects after brain trauma. J. Neurotrauma, 36, 43–53.
- Khan, M.A., Castro-Guerrero, N.A., McInturf, S.A. et al. (2018) Changes in iron availability in Arabidopsis are rapidly sensed in the leaf vasculature and impaired sensing leads to opposite transcriptional programs in leaves and roots. Plant. Cell Environ. 41, 2263–2276.
- Kobayashi, T., Nozoye, T. and Nishizawa, N.K. (2019) Iron transport and its regulation in plants. *Free Radic. Biol. Med.* **133**, 11–20.
- Lalonde, S., Stone, O.A., Lessard, S., Lavertu, A., Desjardins, J., Beaudoin, M., Rivas, M., Stainier, D.Y.R. and Lettre, G. (2017) Frameshift indels introduced by genome editing can lead to in-frame exon skipping. *PLoS One*, 12, e0178700.
- Le, C.T.T., Brumbarova, T., Ivanov, R., Stoof, C., Weber, E., Mohrbacher, J., Fink-Straube, C. and Bauer, P. (2016) ZINC FINGER OF ARABIDOPSIS THALIANA12 (ZAT12) interacts with FER-LIKE IRON DEFICIENCY-INDUCED TRANSCRIPTION FACTOR (FIT) linking iron deficiency and oxidative stress responses. Plant Physiol. 170, 540-557.
- Leclerc, J.L., Lampert, A.S., Diller, M.A., Immergluck, J.B. and Doré, S. (2015) Prostaglandin E2 EP2 receptor deletion attenuates intracerebral hemorrhage-induced brain injury and improves functional recovery. ASN Neuro, 7, 175909141557871.
- Lill, R. (2009) Function and biogenesis of iron–sulphur proteins. Nature, 460, 831–838.
- Lipper, C.H., Paddock, M.L., Onuchic, J.N., Mittler, R., Nechushtai, R. and Jennings, P.A. (2015) Cancer-related NEET proteins transfer 2Fe–2S clusters to anamorsin, a protein required for cytosolic iron-sulfur cluster biogenesis. *PLoS One*, 10, e0139699.
- Love, M.I., Huber, W. and Anders, S. (2014) Moderated estimation of fold change and dispersion for RNA-seg data with DESeg2. *Genome Biol.* **15**, 550.
- Lu, Y. (2018) Assembly and transfer of iron-sulfur clusters in the plastid. Front. Plant Sci. 9, 336.
- Mena, N.P., Urrutia, P.J., Lourido, F., Carrasco, C.M. and Núñez, M.T. (2015) Mitochondrial iron homeostasis and its dysfunctions in neurodegenerative disorders. *Mitochondrion*, 21, 92–105.
- Mittler, R., Darash-Yahana, M., Sohn, Y.S., Bai, F., Song, L., Cabantchik, I.Z., Jennings, P.A., Onuchic, J.N. and Nechushtai, R. (2018) NEET proteins: a new link between iron metabolism, reactive oxygen species, and cancer. *Antioxid. Redox Signal.* 30, 1083–1095.
- Moran, R. (1982) Formulae for determination of chlorophyllous pigments extracted with n, n-dimethylformamide. *Plant Physiol.* **69**, 1376–1381.
- Mou, H., Smith, J.L., Peng, L. et al. (2017) CRISPR/Cas9-mediated genome editing induces exon skipping by alternative splicing or exon deletion. Genome Biol. 18, 108.
- Nechushtai, R., Conlan, A.R., Harir, Y. et al. (2012) Characterization of Arabidopsis NEET reveals an ancient role for NEET proteins in iron metabolism. Plant Cell, 24, 2139–2154.
- Ohama, N., Sato, H., Shinozaki, K. and Yamaguchi-Shinozaki, K. (2017) Transcriptional regulatory network of plant heat stress response. *Trends Plant Sci.* 22, 53–65.
- Przybyla-Toscano, J., Roland, M., Gaymard, F., Couturier, J. and Rouhier, N. (2018) Roles and maturation of iron–sulfur proteins in plastids. *JBIC J. Biol. Inorg. Chem.* **23**, 545–566.
- Rey, P., Becuwe, N., Tourrette, S. and Rouhier, N. (2017) Involvement of Arabidopsis glutaredoxin S14 in the maintenance of chlorophyll content. Plant. Cell Environ. 40, 2319–2332.
- Saha, K., Webb, M.E., Rigby, S.E.J., Leech, H.K., Warren, M.J. and Smith, A.G. (2012) Characterization of the evolutionarily conserved iron-sulfur cluster of sirohydrochlorin ferrochelatase from *Arabidopsis thaliana*. *Bio-chem. J.* 444, 227–237.
- Schuler, M., Rellán-Álvarez, R., Fink-Straube, C., Abadía, J. and Bauer, P. (2012) Nicotianamine functions in the Phloem-based transport of iron to sink organs, in pollen development and pollen tube growth in Arabidopsis. Plant Cell, 24, 2380–2400.

- Selote, D., Samira, R., Matthiadis, A., Gillikin, J.W. and Long, T.A. (2015) Ironbinding E3 ligase mediates iron response in plants by targeting basic helixloop-helix transcription factors. Plant Physiol. 167, 273-286.
- Sengupta, S., Nechushtai, R., Jennings, P.A., Onuchic, J.N., Padilla, P.A., Azad, R.K. and Mittler, R. (2018) Phylogenetic analysis of the CDGSH iron-sulfur binding domain reveals its ancient origin. Sci. Rep. 8, 4840.
- Smith, J.L., Mou, H. and Xue, W. (2018) Understanding and repurposing CRISPR-mediated alternative splicing. Genome Biol. 19, 184.
- Su, L.W., Chang, S.H., Li, M.Y., Huang, H.Y., Jane, W.N. and Yang, J.Y. (2013) Purification and biochemical characterization of Arabidopsis At-NEET, an ancient iron-sulfur protein, reveals a conserved cleavage motif for subcellular localization. Plant Sci. 213, 46-54.
- Sui, T., Song, Y., Liu, Z., Chen, M., Deng, J., Xu, Y., Lai, L. and Li, Z. (2018) CRISPR-induced exon skipping is dependent on premature termination codon mutations. Genome Biol. 19, 164.
- Suzuki, N., Miller, G., Salazar, C. et al. (2013) Temporal-spatial interaction between reactive oxygen species and abscisic acid regulates rapid systemic acclimation in plants. Plant Cell, 25, 3553-3569.
- Tamir, S., Eisenberg-Domovich, Y., Conlan, A.R. et al. (2014) A point mutation in the [2Fe-2S] cluster binding region of the NAF-1 protein (H114C) dramatically hinders the cluster donor properties. Acta Crystallogr. Sect. D Biol. Crystallogr. 70, 1572-1578.
- Tamir, S., Paddock, M.L., Darash-Yahana-Baram, M. et al. (2015) Structurefunction analysis of NEET proteins uncovers their role as key regulators

- of iron and ROS homeostasis in health and disease. Biochim. Biophys. Acta, 1853, 1294-1315.
- Thomine, S. and Vert, G. (2013) Iron transport in plants: better be safe than sorry. Curr. Opin. Plant Biol. 16, 322-327.
- Tissot, N., Robe, K., Gao, F. et al. (2019) Transcriptional integration of the responses to iron availability in Arabidopsis by the bHLH factor ILR3. New Phytol. 223, 1433-1446.
- Viana, V.E., Busanello, C., da Maia, L.C., Pegoraro, C. and Costa de Oliveira, A. (2018) Activation of rice WRKY transcription factors: an army of stress fighting soldiers? Curr. Opin. Plant Biol. 45, 268-275.
- Xing, H.L., Dong, L., Wang, Z.P., Zhang, H.Y., Han, C.Y., Liu, B., Wang, X.C. and Chen, Q.J. (2014) A CRISPR/Cas9 toolkit for multiplex genome editing in plants. BMC Plant Biol. 14, 327.
- Zandalinas, S.I., Sengupta, S., Burks, D., Azad, R.K. and Mittler, R. (2019) Identification and characterization of a core set of ROS wave-associated transcripts involved in the systemic acquired acclimation response of Arabidopsis to excess light. Plant J. 98, 126-141.
- Zhang, X., Henriques, R., Lin, S.S., Niu, Q.W. and Chua, N.H. (2006) Agrobacterium-mediated transformation of Arabidopsis thaliana using the floral dip method. Nat. Protoc. 1, 641-646.
- Zumbrennen-Bullough, K.B., Becker, L., Garrett, L. et al. (2014) Abnormal brain iron metabolism in Irp2 deficient mice is associated with mild neurological and behavioral impairments. PLoS One, 9,